NASA TECHNICAL MEMORANDUM

NASA TM X-3528

IN-71
401220

NASA TM X-3528

INVESTIGATION OF BLADE IMPULSIVE NOISE ON A SCALED FULLY ARTICULATED ROTOR SYSTEM

James Scheiman and Danny R. Hoad

Langley Research Center
and
Langley Directorate,
U.S. Army Air Mobility R&D Laboratory
Hampton, Va. 23665

NATIONAL AERONAUTICS AND SPACE ADMINISTRATION • WASHINGTON, D. C. • JUNE 1977

1. Report No.	2. Government Accession No.	3. Recipient's Catalog No.
NASA TM X-3528		

4. Title and Subtitle	5. Report Date
INVESTIGATION OF BLADE IMPULSIVE NOISE ON A SCALED FULLY ARTICULATED ROTOR SYSTEM	June 1977
	6. Performing Organization Code
7. Author(s)	8. Performing Organization Report No.
James Scheiman and Danny R. Hoad	L-11229
	10. Work Unit No.
9. Performing Organization Name and Address NASA Langley Research Center and Langley Directorate, USAAMRDL Hampton, VA 23665	505-10-26-03
	11. Contract or Grant No.
	13. Type of Report and Period Covered
12. Sponsoring Agency Name and Address National Aeronautics and Space Administration Washington, DC 20546 and U.S. Army Air Mobility R&D Laboratory Moffett Field, CA 94035	Technical Memorandum
	14. Army Project No. 1F161102AH45

15. Supplementary Notes

James Scheiman: Langley Research Center.
Danny R. Hoad: Langley Directorate, U.S. Army Air Mobility R&D Laboratory.

16. Abstract

Helicopter impulsive noise tests were conducted in the Langley V/STOL tunnel with an articulated rotor system. The tests demonstrated that impulsive noise could be simulated for low-speed forward flight with low descent rates and also in the high-speed level flight. For the low forward speed condition, the noise level was highly sensitive to small changes in descent rate. For the high-speed condition, the noise level was increased with an increase in rotor thrust.

17. Key Words (Suggested by Author(s))	18. Distribution Statement
Helicopters Acoustics Rotor Impulsive noise	Unclassified - Unlimited Subject Category 02

19. Security Classif. (of this report)	20. Security Classif. (of this page)	21. No. of Pages	22. Price*
Unclassified	Unclassified	46	$4.00

*For sale by the National Technical Information Service, Springfield, Virginia 22161

INVESTIGATION OF BLADE IMPULSIVE NOISE ON A SCALED FULLY ARTICULATED ROTOR SYSTEM

James Scheiman and Danny R. Hoad*
Langley Research Center

SUMMARY

Helicopter impulsive noise tests were conducted in the Langley V/STOL tunnel. The purpose of these tests were (1) to determine whether blade impulsive noise could be demonstrated in a wind tunnel; (2) to measure the characteristics of the impulsive noise in the near field; and (3) to determine the precise location where the impulse originated in space and thus attempt to define the noise source mechanism.

The test data provided the following results. Impulsive noise can be simulated in the V/STOL tunnel with an articulated rotor helicopter model. The impulsive noise was encountered at relatively low forward speeds at low relative descent rates and also at high-speed level flight. For the low forward speed condition, the noise level was highly sensitive to small changes in descent rate. For the high-speed condition, the noise level was increased with an increase in rotor thrust. The impulsive noise source location could not be determined because of reflections within the test chamber.

INTRODUCTION

Helicopter noise is becoming an increasingly important environmental noise problem both from a civil and military standpoint. Three types of helicopter rotor noise have been identified: (1) rotational noise, (2) broadband noise, and (3) impulsive noise. (See fig. 1.) Of these three noise types, blade impulsive noise, when present, has been described as the most annoying subjectively.

Numerous studies have been conducted concerning helicopter blade impulsive noise. Some of the studies were directed to associating the flight condition with the noise level, others with attenuating the noise source, and others with attempting to identify the source mechanism. Some examples of these studies are listed chronologically in references 1 to 18. All these studies have merit in attempting to decrease the effects of blade impulsive noise. For example, by associating the flight condition with the noise intensity, helicopter operation can be restricted or limited to flight conditions where the impulsive noise is minimized. It has been generally accepted, and there is some convincing evidence, that blade impulsive noise is associated with a blade encountering a blade tip vortex shed from a previous blade.

*Langley Directorate, U.S. Army Air Mobility R&D Laboratory.

Therefore, numerous blade-tip shapes (that could affect the shed vortex characteristics) have been acoustically evaluated. (See refs. 2, 4, 5, 7, 11, 13, and 15.) Some of these have proved to be somewhat effective in reducing blade impulsive noise, but the mechanism, or mechanisms, causing impulsive noise is not well understood.

There is little positive information as to the mechanisms that create impulsive noise. For example, references 1, 2, and 14 indicate that blade impulsive noise is associated with blade section stall; references 5 and 8 indicate that the impulsive noise is associated with local blade section compressibility; and other references (for example, ref. 9) indicate that the impulsive noise is associated with the average blade loading and blade tip Mach number. Local blade compressibility could occur either on the advancing blade tip (with adequate Mach number and section angle of attack) or possibly at less stringent conditions with a tip-vortex encounter. Based on available published data (refs. 16, 17, and 18), blade impulsive noise may be produced by various mechanisms: local compressibility (refs. 5 and 8), local blade stall (refs. 1, 2, and 14), and rapid change in local blade section angle of attack. These source mechanisms can occur with or without a tip-vortex encounter as suggested in reference 16. Certainly the proximity of a tip vortex could encourage, intensify, or bring on the mechanism earlier than without the tip-vortex encounter.

The purpose of this investigation was to determine whether the blade impulsive noise could be demonstrated in a wind tunnel, to measure the characteristics of the impulsive noise in the near field, and to determine the precise location where the impulse originated in space. The tests were conducted in the Langley V/STOL tunnel by using a general rotor model system with a four-blade articulated rotor system. The model was tested at a constant rotational speed with a varying forward speed, angle of attack, and thrust condition.

SYMBOLS

The units used for physical quantities defined in this paper are given in both the U.S. Customary Units and the International System of Units. Factors relating these two systems of units are presented in reference 19. The symbols are defined as follows; the symbols enclosed in parentheses are used in table 1 and their usual notation precedes them.

b number of blades

c rotor blade chord, m (ft)

$\frac{C_H}{\sigma}$ (CH) rotor drag-force coefficient, $\frac{H}{\rho\sigma\pi R^2 V_T^2}$

$\frac{C_T}{\sigma}$ (CT) rotor thrust coefficient, $\frac{T}{\rho\sigma\pi R^2 V_T^2}$

$\frac{C_Y}{\sigma}$ (CY) rotor side-force coefficient, $\frac{Y}{\rho\sigma\pi R^2 V_T{}^2}$

H rotor drag force normal to control axis, N (lbf)

q (Q) free-stream dynamic pressure, Pa (lbf/ft^2)

R rotor disk radius, m (ft)

SPL sound pressure level, dB

SPL_n normalized sound pressure level, dB

T rotor thrust alined with control axis, N (lbf)

V free-stream velocity, m/sec (ft/sec)

V_T (VT) rotor blade rotational tip speed, m/sec (ft/sec)

X,Y,Z coordinate axes

x longitudinal position of microphones or rotor (see fig. 3), cm (in.)

Y rotor side force normal to control axis, N (lbf)

y lateral position of microphones or rotor (see fig. 3), cm (in.)

z vertical location of microphones or rotor (see fig. 3), cm (in.)

α angle of attack of fuselage, deg

α_c (ALPHAC) angle of attack of control axis, positive when nose is up, deg

δ_3 pitch-flap coupling angle, deg

θ (TC(0)) rotor blade root collective pitch angle, deg

ρ (RHO) free-stream density, kg/m^3 ($slugs/ft^3$)

σ rotor solidity, $bc/\pi R$

APPARATUS AND METHODS

The General Rotor Model System (GRMS) with a four-blade articulated hub was tested in the Langley V/STOL tunnel to demonstrate and evaluate blade impulsive noise.

The V/STOL wind tunnel has a test section that is 4.42 m (14.50 ft) high and 6.63 m (21.75 ft) wide. To minimize acoustic wall reflections during the acoustic tests, the walls were removed and the ceiling was raised to its maximum height, which was about 9.4 m (31 ft) above the center of the rotor rotation system. In addition, the floor and ceiling slots, which represent about 10 percent of the surface area, were opened.

Model Description and Installation

A photograph of the model is shown in figure 2. A three-view drawing of the model and the setup is shown in figure 3. The auxiliary thrust engines of the model were in place but not operating.

The model was a four-blade articulated rotor with a diameter of 3.127 m (10.26 ft). The blades had no twist and the airfoil was an NACA 0012 section (table 2). The blade pitch-flapping angle δ_3 was -2.0°. The rotor was driven by two water-cooled electric motors that could each produce up to 67 kW (90 hp). It was operated at nearly constant rotational speed between 1280 and 1292 revolutions per minute, which resulted in a rotational tip speed of 213.4 m/sec (700 ft/sec).

The blade-tip shape was a body of revolution with a revolution radius equal to the blade thickness at each chord station. The rotor blade pitch control system which provided cyclic and collective controls consisted of a swash plate which was driven by remotely controlled electric motors. Details of the helicopter rotor dimensions are listed in table 2.

The present test utilized data from two strain-gage force balances. One balance was attached to the rotor system and measured the forces and moments on the rotor only. The other balance was fastened between the fuselage and sting; this balance measured the forces and moments on the entire model. Additional information about the balance system or model can be found in reference 20.

The model was mounted on a sting in the wind tunnel. The sting is capable of wide variations of roll and pitch angles about a fixed point in the wind tunnel. For these tests, the fixed point, which was 0.60 m (1.99 ft) below the center of rotor rotation, was 2.92 m (9.58 ft) above the tunnel floor. The fuselage roll angles were kept at 0°.

Acoustic Instrumentation and Recording System

The acoustic sensors consisted of eight 1.27-cm-diameter (0.50-in.) condenser microphones. A schematic drawing of the acoustic instrumentation system is shown in figure 4. The recording system consisted of an amplifier-attenuator system and a 14-channel frequency-modulated (FM) magnetic tape recorder.

Six of the eight microphones were located near the plane of the rotor. The microphone locations and their coordinates are shown in figure 3. Microphones 4, 5, and 6 were located on the advancing side of the rotor and microphones 1, 2, and 3 on the retreating side. These microphones were located relatively close to the blade tips (in the acoustic near field) so that direct rotor noise would dominate the reflected noise. Some of these microphones and the microphone stands can be seen in the photograph in figure 2. Microphones 7 and 8 were mounted flush with the wind-tunnel floor, one under the advancing side of the rotor and one under the retreating side. A schematic of the test setup can be seen in figure 5.

The strain-gage balance signals, rotor control system positions, blade flapping, and fuselage attitude were collected and the data were numerically operated on by an on-line computer-controlled data acquisition system.

Operating Procedures and Test Conditions

During these tests, a constant tunnel speed was used during rotor angle-of-attack sweeps. The speeds used were 30.86, 36.01, 41.16, 46.30, 56.59, and 61.73 m/sec (101.2, 118.1, 135.0, 151.8, 185.6, and 202.4 ft/sec). At each rotor angle-of-attack position, the rotor controls were varied with the guidance of the on-line data acquisition system to obtain balanced rotor forces. After the rotor controls were set, the microphone-signal amplifiers were adjusted and the acoustic signals recorded on the magnetic tape recorder. The test conditions shown in table 1 include all rotor operating conditions where acoustic data were obtained. The operating conditions include three components of rotor forces with respect to the control axes, the control pitch angles, and the tunnel operating conditions. The rate of descent was determined from the lift-drag ratio.

In addition to the rotor noise measurements, tests were conducted with a known impulsive noise source to verify the capability of determining the source location from the acoustic data. For these tests, a gun was fired at various known locations within the microphone array, and the results were simultaneously recorded on the magnetic tape recorder.

Before and after the tests, "pink" and "white" noise signals were recorded through the recording system. A pink noise signal has a frequency amplitude spectrum such that a one-third octave band analysis will result in a nearly constant output for each band. A white noise signal has a frequency amplitude spectrum with a constant output when subjected to a narrow (constant band width) band analysis. The purpose of these input signals was to calibrate the complete system (including the data-reduction equipment) frequency response. All microphones were calibrated with a 114-dB calibrator at 1000 Hz before and after each series of tests in order to verify the stability of the system.

DATA REDUCTION

The acoustic data were analyzed for one-third-octave and narrow-band sound pressure levels, and the recorded microphone data were crosscorrelated to determine the time delay between microphones for the arrival of the blade slap signal. The one-third-octave band data analysis was performed by use of a set of electronic filters. The narrow-band analysis was performed with a constant band width of 21.5 Hz and a 2-second real-time averaging. No corrections for microphone response, background noise level, or reverberations were applied to the data. A typical system response curve (excluding microphones) for these different input levels is shown in figure 6. Because of the responce characteristics of the microphones used, the amplitude drops off very rapidly for frequencies above 20 kHz. The wind-tunnel noise dominated all other acoustic levels for frequencies below about 50 Hz.

To minimize the effect of the time lag in the tape recorder recording head, microphones 1 to 6 were recorded on even numbered channels. Before attempting any crosscorrelation between tape recorder channels, this instrument time lag was investigated and was found to be a few microseconds. Various combinations of two spacially separated microphones were correlated in order to determine the time lag between arrivals of each impulsive signal. The first signals correlated were the gun shots where the signal source location was known. In addition, oscillograph records were made of the acoustic signals and the time delays between microphones determined by analysis of the physical measurements from the records. With these time delays and using triangulation, the impulse noise location was determined. The first estimate of the source location (using triangulation) neglected the tunnel speed effects on the acoustic signal.

In addition to the acoustic data presented in table 1, the rotor performance data determined from the force balances are presented.

RESULTS AND DISCUSSION

The procedure used herein to determine the source mechanism of helicopter impulsive noise was to operate the rotor system in the different regions where blade impulsive noise is likely to occur, determine the physical source location in space, and then attempt to explain what was happening at that location that could cause the noise.

One possible mechanism is related to blade operation in the presence of a tip vortex shed from a previous blade. The rotor operating condition chosen for investigation of this phenomena was a partial-power descent. For these tests, the rotor was operated at a constant forward speed at various simulated descent rates and thrust conditions. Another possible mechanism is related to local blade section compressibility. The rotor was operated in level flight at the highest possible advancing blade tip Mach numbers to investigate the phenomena. For these high-speed test conditions, the thrust variable was evaluated.

Background noise measurements were made at various tunnel speeds with the model minus the rotor blades in the tunnel and without the rotor drive motor operating. The acoustic data were normalized by using the V^6 law (see ref. 21) and superimposing all the data for the different speeds. Figure 7 presents the resulting maximum and minimum normalized sound pressure levels of the superimposed results for three microphones. The data for microphones 7 and 8 for the different tunnel speeds nearly coincide. The data for microphone 3 had some tones whose frequencies were velocity dependent as evidenced by the relatively large variations in maximum and minimum levels for microphone 3 between frequency bands of 1.25 kHz and 4 kHz in figure 7. Figure 8 presents a narrow-band analysis of background noise for microphone 3 at a 30.2-m/sec (99-ft/sec) tunnel speed. Note the pure tones at 6 kHz and

8 kHz which are possibly related to the microphone stand tie-down cables. In addition to the normalized data in figure 7, the measured background sound pressure level data for a tunnel speed of 30.2 m/sec (99 ft/sec) are presented on some of the spectrums in figure 9. For example, figures 9(b) and 9(e) show that the measured rotor noise was significantly above the background noise level. During the test, the occurrence of impulsive noise could be seen in the on-line time history display (see fig. 9), and the change in the audible characteristics of the noise transmitted to the control station was easily discernible.

The results of these tests are presented in three sections: (1) forward speed with descent; (2) high-speed level flight; and (3) noise source location.

Forward Speed With Descent

Table 1 presents the test parameters for the rotor operating conditions. The test points for tables 1(a) to 1(d) and 1(f) to 1(h) are from test runs with a nearly constant thrust and a variable descent rate (rotor attitude) for points within the run. The test points in tables 1(e) to 1(i) are for a nearly constant descent rate at various total-thrust levels. Test points in tables 1(j), 1(k), and 1(l) are the high-speed runs that will be discussed in a later section. Note that the blade rotational tip speed was nearly constant at 213.4 m/sec (700 ft/sec) and that the control axis was the reference axis for the appropriate variables.

To explore blade impulsive noise for the descent mode of helicopter operation, oscillograph records and frequency spectrums were made. Data shown in figure 9 are for a constant forward speed of 30.2 m/sec (99 ft/sec) and various descent rates to map out the expected intense noise region. The upper part of each plot in figure 9 is a sample trace of the sound pressure time history. Note that the amplitude scale on the oscillograph traces are not all the same. The lower part of the figure is a one-third-octave spectrum analysis of the same data. Figure 9 includes data for two microphones on the retreating side of the rotor (microphones 2 and 3), two microphones on the advancing side (microphones 4 and 6), and one miocrophone in the tunnel floor (microphone 8). The rotor rotational speed was about 1290 revolutions per minute which, for a four-blade rotor, resulted in a blade passage frequency of about 86 Hz. On a one-third-octave spectrum, this frequency is in the 80-Hz band, and the second harmonic is in the 160-Hz band. All microphones in figure 9 show an indication of blade passage frequency on the oscillograph or spectrum plots.

The large variations in the sound pressure level in figure 9(d) (microphone 6) for frequencies below 80 Hz indicate that this microphone was in the rotor downwash. In fact, some of the oscillograph records for this microphone showed two blade passage peaks, one for the blade and one, immediately following, for the pressure variations within the downwash caused by the blade passage.

A typical oscillograph record of blade passage without blade slap is shown on the lowest trace (descent speed of 8.35 m/sec (27.38 ft/sec)) in figure 9(b). The blade impulsive noise is superimposed on the blade passage noise; this effect is shown on the second and third trace (descent speeds of 4.84 and 5.14 m/sec (15.88 and 16.86 ft/sec)) in figures 9(c) and 9(d). Since time and blade azimuth angle are increasing from left to right, the impulsive noise occurs just prior to the blade passage. Thus, it might be concluded that the impulsive noise occurs around a blade azimuth position of about 70°. Blade azimuth of 0° is defined as the blade in the downstream position.

When analyzing acoustic data from an extended source region, a determination must be made as to whether the microphones are in the acoustic far field or near field. The definition of near and far field is, however, not precise. It is generally defined by the model component size and the maximum wavelength of the acoustic frequencies of interest. The determination of the transition point between near and far field is typically defined in terms of multiples of wavelength and model component size. The multiples normally used range from two to ten. The microphone will be considered to be in the far field when it is farther from the source than five times the maximum wavelength of interest. By using the blade chord (10.7 cm (4.25 in.)) and the wavelength for a frequency of 500 Hz, it can be seen from figure 3 that microphones 1 to 6 are in the near field and the data should be interpreted as such. However, microphones 7 and 8 are in the far field when these criteria are used.

A narrow-band analysis (21.5-Hz bandwidth) was performed on a limited amount of the data to obtain a more detailed spectrum of the impulsive noise. A typical spectrum is presented in figure 10 for microphone 3 and for four descent rates. The narrow-band data in figure 10 is the same data as the one-third-octave data presented in figure 9(b). The background noise level for the data in figure 10 is shown in figure 8. In general, the sound pressure levels in figure 10 are above those in figure 8. However, figure 10(d) indicates the presence of a pure tone at about 5.5 kHz which is part of the background noise in figure 8.

As will be shown in figure 11, each microphone spectrum in figure 9 and the spectra in figure 10 are for rotor operation at descent rates surrounding those of the most intense impulsive noise region. By comparing figure 9(b) with figure 10, it is seen that many more harmonics of blade passage frequency are seen in the narrow band than in the one-third-octave band presentations. The difference in the spectra indicates the area where the impulsive noise sound energy is concentrated. In figure 10 the sound pressure levels for descent rates of 4.84 and 5.14 m/sec (15.88 and 16.9 ft/sec) are higher than those for 1.94 and 8.35 m/sec (6.45 and 27.4 ft/sec). This result implies more intense impulsive noise for these descent rates. Furthermore, there are many more harmonics of blade passage frequencies when the impulsive noise is present (figs. 10(b) and 10(c)). The narrow-band analysis was performed by averaging over a number of rotor revolutions. Since the impulsive noise occurs at a blade passage frequency, a frequency analysis would naturally result in harmonics of blade passage.

The data in figures 9 and 10 indicate that most of the blade impulsive noise occurs at frequencies above about 500 Hz, and, as discussed earlier, microphones 1 to 6 can be considered in the near field and microphones 7 and 8 in the far field. In order to keep the blade rotational noise (see fig. 1) from affecting the blade impulsive noise overall sound pressure data (see, for example, figs. 9(b), 9(c), 9(d), 10(b), or 10(c)), a 500-Hz high-pass filter was used. Figure 11 presents isobars of filtered overall sound pressure level maps for various forward and descent speeds. Contour maps for two microphones are shown, one microphone near the rotor disk and one in the floor. The contour maps for the other microphones (not shown) are very similar. These data are presented to show that an articulated rotor model in the V/STOL tunnel could be used to investigate helicopter blade impulsive noise.

The data in figure 11 are similar to other published data showing that for certain combinations of forward and descent speeds, the blade impulsive noise is more intense than that for other speed combinations. (See, for example, ref. 18.) The wind-tunnel background noise varies with forward speed; however, with a 500-Hz filter as in figure 11, most of the tunnel drive noise is filtered out. Therefore, for figure 11, the lowest level shown can be conservatively assumed to be the background noise. The data show that additional tests at lower forward velocities are needed to complete the sound pressure maps for the maximum intensity contour.

The contour plots indicate that the noise gradients are much higher for variations in descent speed than for variations in forward speed. A descent-speed variation of a few meters per second resulted in a 5- to 10-dB variation in sound pressure level; whereas, it required a 20 m/sec (65.6 ft/sec) or more variation in forward speed to achieve the same change in sound pressure level. The forward speed affects the lateral position of the rotor shed tip vortex; whereas, the descent rate affects the vertical position of the tip vortex. As indicated in the literature and as implied herein, blade impulsive noise in rotor descent operation is related to blade tip vortex interaction. However, the mechanism that creates the impulsive noise (local compressibility, stall, or pressure fluctuation) is still unknown.

High-Speed Level Flight

A rather severe form of blade impulsive noise can be associated with high advancing blade tip Mach numbers. This type of impulsive noise has been shown to occur when the local Mach number on the blade reaches critical conditions and shock waves occur which can be related to local blade section lift and drag divergence. (See ref. 22.) In an attempt to generate local critical Mach number conditions, the rotor system was operated at a high forward speed (56.59 m/sec (185.6 ft/sec)) through a range of thrust coefficients. Preliminary qualitative noise levels at higher speeds up to and including the maximum speed considered safe for rotor operation indicated that the rotor noise level was at or above the background noise level. With the maximum rotor rotational speed of 1300 rpm, the maximum corresponding advancing tip Mach number was approximately 0.8. The variation in thrust was an attempt to achieve local critical Mach number conditions. These test conditions are presented in tables 1(j) to 1(l).

Figure 12 presents the one-third-octave sound pressure level spectrum measured by the eight microphones for this attempt at generating the high-speed noise source. The signal-to-noise ratio of these data (see fig. 12(c)) is rather low, and an analysis of rotor noise should be made with the realization that the data are contaminated by background noise. In particular, the variation of sound pressure level with thrust at one-third-octave band of 3.15 kHz is virtually nonexistent. This condition indicates that the noise level is not related to the test model variables, but to a relatively high ambient level. Another example of high background noise level can be seen by examining the spectra at low thrust levels. Across the spectrum the change in sound pressure level with increasing thrust (C_T/σ = 0.040 to 0.063) is negligible; thus, the background noise is predominant. At higher thrust coefficients, however, useful trends can be extracted from these data.

The data in figure 12 indicate that the noise radiated to the microphones is highest in blade passage frequency band. Since the only model parameter variable for these test cases is the rotor thrust, it must be the source of the variation in sound pressure level. The increasing sound pressure level with increasing thrust indicates a trend. The data presented for microphone 6 (fig. 12(f)), however, does not follow this trend completely. As discussed before, this microphone is subjected to rotor downwash turbulence in some rotor flight conditions; therefore, the anomalies in figure 12(f) could be attributed to what is called pseudo-sound (pressure fluctuations generated by turbulent flow over the microphone).

For frequencies above 500 Hz, figure 12 indicates the dependence of sound pressure level with thrust. If it is recalled that the characteristics of the blade-vortex interaction noise was predominant above 500 Hz, the results presented in figure 12 indicate that this proportionality of sound pressure level against thrust of the high-speed noise can be attributed to an impulsive noise source. As done previously, the data presented in figure 12 were high pass filtered at 500 Hz, and the overall sound pressure level was determined. These overall sound pressure levels are presented in figure 13 as a function of the rotor thrust level. This figure shows that impulsive noise level varies with microphone or rotor azimuth position. Figure 13 also shows that this impulsive noise does increase with increasing thrust at each microphone location. It is believed, however, that local critical Mach number conditions were just barely met at the blade tip in these tests and that further increases in rotor speed and/or further increases of thrust would immerse the tip in the local critical Mach number condition and create very intense impulsive noise characteristics. An extension of the tests would undoubtedly provide data that would better substantiate these conclusions.

Noise Source Location

One of the primary purposes of these noise tests was to determine the impulsive noise source location. With the location known, the operating conditions on the blade could be computed and a noise mechanism postulated.

Some limited, but special, tests were conducted in order to evaluate and verify the technique for determining source location. These tests consisted of firing a handgun, which produces a high-amplitude point-source noise, at known locations within the microphone array. The object was to compute the source location from the recorded microphone signals and to compare the computed location with the specific physical location. After some data reduction technique development, the gun firing location was determined from the recorded acoustic data.

With the rotor operating in a blade slap condition, attempts were made to determine noise signal time delays by crosscorrelating two microphone outputs. However, numerous problems were encountered, the wall reflections being foremost; and the attempts to determine the impulsive noise source location were unsuccessful.

CONCLUSIONS

Tests were conducted in the Langley V/STOL tunnel with a four-blade articulated helicopter rotor system to evaluate helicopter blade impulsive noise. The tests were to determine (1) the possibility of simulating blade impulsive noise in the V/STOL tunnel; (2) the operating conditions associated with the noise levels; and (3) the possible noise mechanisms. The conclusions for this study are as follows:

1. Helicopter blade impulsive noise can be simulated in the V/STOL tunnel with an articulated rotor system.

2. Blade impulsive noise was encountered at the low forward speeds at the slow descent rate and also at high-speed level-flight conditions (56.6 m/sec (185.6 ft/sec)).

3. The impulsive noise for both the low and high forward speed conditions appeared at frequencies above about 500-Hz model scale. (Blade passage frequency was nearly constant at about 86 Hz.)

4. For the low forward speed and low descent rate rotor operating conditions, the noise level was highly sensitive to small changes in descent rate and much less sensitive to changes in forward speed.

5. For the high-speed flight condition at 56.6 m/sec (185.6 ft/sec), the blade impulsive noise level increased with increase in rotor thrust coefficient and the level varied with rotor azimuth position.

6. There is some evidence that the impulsive noise originates on the advancing side of the rotor.

Langley Research Center
National Aeronautics and Space Administration
Hampton, VA 23665
April 28, 1977

REFERENCES

1. Schlegel, Ronald; King, Robert; and Mull, Harold: Helicopter Rotor Noise Generation and Propagation. USAAVLABS Tech. Rep. 66-4, U.S. Army, Oct. 1966.

2. Schlegel, Ronald G.; and Bausch, William E.: Helicopter Rotor Noise Prediction and Control. No. 209, 24th Annual National Forum Proceedings, American Helicopter Soc., Inc., May 1968.

3. Sternfeld, Harry, Jr.; and Spencer, Robert H.: Recent Research in Rotor-Noise Reduction. [Preprint] 690684, Soc. Automot. Eng., Oct. 1969.

4. Spivey, W. A.; and Morehouse, G. G.: New Insights Into the Design of Swept-Tip Rotor Blades. Preprint No. 420, American Helicopter Soc., June 1970.

5. Arndt, Roger E. A.; and Borgman, Dean C.: Noise Radiation From Helicopter Rotors Operating at High Tip Mach Number. No. 402, 26th Annual National Forum Proceedings, American Helicopter Soc., Inc., June 1970.

6. Widnall, S.: Helicopter Noise Due to Blade-Vortex Interaction. J. Acoust. Soc. America, vol. 50, pt. 2, July 1971, pp. 354-365.

7. Leverton, J. W.: The Sound of Rotorcraft. Aeronaut. J. Roy. Aeronaut. Soc., vol. 75, no. 726, June 1971, pp. 385-397.

8. Sternfeld, H.; Spencer, R. H.; and Schairer, J. O.: An Investigation of Noise Generation on a Hovering Rotor. Doc. D210-10229-1, Boeing Co., Jan. 1971. (Available from DDC as AD 721 312.)

9. Bausch, W. E.; Munch, C. L.; and Schlegel, R. G.: An Experimental Study of Helicopter Rotor Impulsive Noise. USAAVLABS Tech. Rep. 70-72, U.S. Army, June 1971.

10. Gray, Robin B.; and Pierce, G. Alvin: Exploratory Investigation of Sound Pressure Level in the Wake of an Oscillating Airfoil in the Vicinity of Stall. NASA CR-1948, 1972.

11. Pollard, J. S.; and Leverton, John W.: Effect of Blade Tip Planform on the Noise and Aerodynamics of a Helicopter Rotor. Res. Paper 414, Westland Helicopters Ltd., Apr. 24, 1972.

12. Sternfeld, H., Jr.: Acoustical Modeling of the Heavy Lift Helicopter. Proceedings of Symposium on Status of Testing and Modeling Techniques for V/Stol Aircraft, American Helicopter Soc., Oct. 1972.

13. Tangler, James I.; Wohlfeld, Robert M.; and Miley, Stan J.: An Experimental Investigation of Vortex Stability, Tip Shapes, Compressibility, and Noise for Hovering Model Rotors. NASA CR-2305, 1973.

14. Paterson, Robert W.; Amiet, Roy K.; and Munch, C. Lee: Isolated Airfoil - Tip Vortex Interaction Noise. AIAA Paper No. 74-194, Jan.-Feb. 1974.

15. Tangler, James L.: The Design and Testing of a Tip To Reduce Blade Slap. Preprint No. 973, 31st Annual National Forum, American Helicopter Soc., May 1975.

16. Vause, C. R.; Schmitz, F. H.; and Boxwell, D. A.: High-Speed Helicopter Impulsive Noise. Preprint No. 1004, Proceedings of the 32nd Annual National V/STOL Forum, American Helicopter Soc., Inc., May 1976.

17. Shockey, G. A.; Williamson, J. W.; and Cox, C. R.: Helicopter Aerodynamics and Structural Loads Survey. Preprint No. 1060, Proceedings of the 32nd Annual National V/STOL Forum, American Helicopter Soc., May 1976.

18. Schmitz, F. H.; and Boxwell, D. A.: In-Flight Far-Field Measurement of Helicopter Impulsive Noise. Preprint No. 1062, Proceedings of the 32nd Annual National V/STOL Forum, American Helicopter Soc., Inc., May 1976.

19. Mechtly, E. A.: The International System of Units - Physical Constants and Conversion Factors (Second Revision). NASA SP-7012, 1973.

20. Wilson, John C.: A General Rotor Model System for Wind-Tunnel Investigation of Rotorcraft Aerodynamics and Acoustics. Proceedings 9th Aerodynamic Testing Conference (Arlington, Texas), June 1976.

21. Vér, István L.: Acoustical Evaluation of the NASA Langley V/Stol Wind Tunnel. NASA CR-145087, [1976].

22. Abbott, Ira H.; and Von Doenhoff, Albert E.: Theory of Wing Sections. Dover Publ., Inc., c.1959.

TABLE 1.- ROTOR TEST CONDITIONS

(a) $Q \approx 570\ N/m^2\ (11.9\ lb/ft^2)$, $CT \approx 0.063$

ALPHAC	TC(0)	VT	PHO	Q	----CONTROL---- CT	CH	CY
-.39	-.06	213.1 (699.)	1.228 (.0023819)	4.7 (.098)	.00070	-.00005	-.00012
-.04	6.52	212.6 (698.)	1.236 (.0023977)	554.5 (11.580)	.06246	.00259	.00102
-1.18	5.83	212.7 (698.)	1.230 (.0023869)	570.0 (11.904)	.05480	.00185	.00056
-1.16	6.32	212.7 (698.)	1.227 (.0023816)	566.4 (11.829)	.05987	.00220	.00077
-2.24	6.44	213.2 (699.)	1.222 (.0023719)	565.9 (11.819)	.06067	.00203	.00080
-3.33	6.65	212.6 (698.)	1.221 (.0023690)	568.9 (11.882)	.06221	.00196	.00087
-4.42	6.88	212.5 (697.)	1.219 (.0023649)	569.4 (11.893)	.06427	.00182	.00109
-5.51	7.01	213.1 (699.)	1.224 (.0023759)	574.4 (11.997)	.06447	.00178	.00097
-6.06	7.09	212.5 (697.)	1.232 (.0023911)	572.8 (11.964)	.06480	.00172	.00107
-.56	-.06	213.2 (699.)	1.236 (.0023985)	4.6 (.096)	.00127	-.00009	-.00007

(b) $Q \approx 560\ N/m^2\ (11.7\ lb/ft^2)$, $CT \approx 0.064$

ALPHAC	TC(0)	VT	PHO	Q	----CONTROL---- CT	CH	CY
-.31	-.06	212.7 (698.)	1.239 (.0024034)	4.7 (.098)	.00057	-.00000	-.00011
-.00	6.65	212.7 (698.)	1.228 (.0023823)	553.0 (11.549)	.06468	.00296	.00114
1.08	6.53	212.6 (697.)	1.223 (.0023726)	562.3 (11.745)	.06510	.00321	.00126
2.19	6.41	212.8 (698.)	1.221 (.0023692)	559.5 (11.685)	.06556	.00343	.00117
3.12	6.19	212.7 (698.)	1.235 (.0023965)	571.1 (11.927)	.06349	.00344	.00097
4.30	5.97	212.9 (699.)	1.240 (.0024064)	564.9 (11.799)	.06233	.00345	.00077
-.71	-.05	213.1 (699.)	1.234 (.0023947)	4.5 (.095)	.00166	-.00022	.00007

(c) $Q \approx 560\ N/m^2\ (11.7\ lb/ft^2)$, $CT \approx 0.058$

ALPHAC	TC(0)	VT	PHO	Q	----CONTROL---- CT	CH	CY
-.30	-.05	210.0 (689.)	1.228 (.0023821)	4.7 (.098)	.00059	.00001	-.00015
-2.40	4.77	212.9 (698.)	1.231 (.0023887)	566.9 (11.840)	.04228	.00144	-.00016
2.80	4.76	212.6 (698.)	1.238 (.0024021)	550.9 (11.505)	.05542	.00180	.00070
3.91	4.94	212.5 (697.)	1.241 (.0024070)	560.4 (11.705)	.05906	.00227	.00099
5.01	4.81	212.6 (697.)	1.238 (.0024023)	556.5 (11.622)	.05936	.00253	.00102
6.11	4.71	212.9 (698.)	1.234 (.0023947)	557.7 (11.647)	.05917	.00274	.00087
7.21	4.61	212.8 (698.)	1.234 (.0023953)	559.0 (11.674)	.05852	.00299	.00054
8.29	4.49	213.2 (699.)	1.225 (.0023775)	566.4 (11.829)	.05904	.00316	.00048
9.35	4.38	213.1 (699.)	1.225 (.0023767)	562.6 (11.749)	.05852	.00342	.00019

TABLE I.- Continued

(d) $Q \approx 568$ N/m^2 (11.8 lb/ft^2), $CT \approx 0.057$

ALPHAC	TC(0)	VT	RHO	Q	----CONTROL---- CT	CH	CY
-.25	-.07	213.1 (699.)	1.229 (.0023847)	4.7 (.098)	.00047	.00000	-.00018
5.78	3.96	212.7 (698.)	1.243 (.0024112)	576.7 (12.044)	.05803	.00169	.00083
6.86	3.84	212.7 (698.)	1.243 (.0024115)	570.1 (11.906)	.05753	.00182	.00085
7.96	3.73	213.0 (699.)	1.240 (.0024057)	570.9 (11.924)	.05701	.00211	.00069
9.07	3.61	212.6 (697.)	1.235 (.0023958)	567.0 (11.843)	.05738	.00246	.00085
10.16	3.48	212.7 (698.)	1.231 (.0023887)	566.1 (11.824)	.05596	.00267	.00059
11.27	3.48	213.0 (699.)	1.227 (.0023817)	564.7 (11.794)	.05760	.00296	.00053
12.36	3.47	212.8 (698.)	1.228 (.0023824)	558.0 (11.654)	.05772	.00318	.00028

(e) $Q \approx 785$ N/m^2 (16.4 lb/ft^2), $CT \approx 0.060$

ALPHAC	TC(0)	VT	RHO	Q	----CONTROL---- CT	CH	CY
8.15	4.54	212.6 (698.)	1.242 (.0024096)	771.3 (16.109)	.07622	.00359	.00156
8.05	3.71	212.7 (698.)	1.241 (.0024075)	785.6 (16.409)	.06582	.00303	.00099
8.00	3.21	212.7 (698.)	1.235 (.0023970)	791.0 (16.521)	.05987	.00263	.00076
9.11	3.12	212.7 (698.)	1.232 (.0023897)	789.7 (16.494)	.06068	.00324	.00081
10.21	2.99	213.1 (699.)	1.228 (.0023831)	791.3 (16.527)	.06069	.00345	.00073

(f) $Q \approx 795$ N/m^2 (16.6 lb/ft^2), $CT \approx 0.059$

ALPHAC	TC(0)	VT	RHO	Q	----CONTROL---- CT	CH	CY
2.86	4.57	212.6 (697.)	1.239 (.0024040)	789.7 (16.493)	.06059	.00255	.00091
3.98	4.44	212.8 (698.)	1.241 (.0024076)	799.5 (16.697)	.06048	.00294	.00082
5.03	4.24	213.1 (699.)	1.240 (.0024058)	789.8 (16.496)	.05934	.00318	.00088
6.11	4.01	212.9 (698.)	1.236 (.0023975)	793.6 (16.574)	.05843	.00331	.00068
2.86	4.47	212.2 (696.)	1.230 (.0023875)	794.7 (16.597)	.05955	.00251	.00080
1.74	4.59	212.4 (697.)	1.228 (.0023820)	799.0 (16.688)	.05937	.00245	.00090
.67	4.71	212.4 (697.)	1.226 (.0023786)	799.9 (16.706)	.05899	.00223	.00097

(g) $Q \approx 1015$ N/m^2 (21.2 lb/ft^2), $CT \approx 0.059$

ALPHAC	TC(0)	VT	RHO	Q	----CONTROL---- CT	CH	CY
1.82	4.98	212.7 (698.)	1.214 (.0023559)	1016.4 (21.229)	.06889	.00349	.00127
.69	4.79	212.6 (698.)	1.222 (.0023702)	1018.4 (21.271)	.06341	.00287	.00115
-.43	4.61	212.7 (698.)	1.227 (.0023800)	1015.3 (21.204)	.05861	.00249	.00103
.64	4.49	212.7 (698.)	1.229 (.0023848)	1018.3 (21.267)	.05934	.00271	.00095
1.72	4.28	212.8 (698.)	1.229 (.0023847)	1023.7 (21.380)	.05949	.00297	.00085
2.82	4.15	212.8 (698.)	1.226 (.0023792)	1012.8 (21.152)	.05951	.00312	.00072
3.91	3.93	212.8 (698.)	1.223 (.0023727)	1015.1 (21.201)	.05959	.00336	.00069
5.02	3.82	212.9 (698.)	1.219 (.0023647)	1013.4 (21.166)	.06042	.00374	.00078

TABLE 1.- Continued

(h) $Q \approx 1297\ N/m^2\ (27.1\ lb/ft^2)$, $CT \approx 0.062$

ALPHAC	TC(0)	VT	RHO	Q	----CONTROL---- CT	CH	CY
-.35	5.02	212.9 (698.)	1.209 (.0023454)	1297.5 (27.100)	.06840	.00397	.00146
-.39	4.63	212.6 (698.)	1.212 (.0023520)	1301.9 (27.190)	.06320	.00355	.00112
.66	4.39	212.8 (698.)	1.216 (.0023602)	1302.4 (27.201)	.06199	.00364	.00104
1.74	4.19	212.7 (698.)	1.221 (.0023685)	1298.5 (27.119)	.06189	.00387	.00087
2.83	3.96	213.0 (699.)	1.222 (.0023717)	1296.8 (27.085)	.06229	.00404	.00076
3.90	3.65	212.6 (697.)	1.223 (.0023723)	1296.7 (27.083)	.06073	.00413	.00064
4.99	3.31	212.9 (698.)	1.220 (.0023667)	1292.9 (27.004)	.06007	.00435	.00059

(i) $Q \approx 782\ N/m^2\ (16.3\ lb/ft^2)$, $CT \approx$ Variable

ALPHAC	TC(0)	VT	RHO	Q	----CONTROL---- CT	CH	CY
-1.46	4.11	212.5 (697.)	1.207 (.0023428)	794.2 (16.587)	.04658	.00218	.00053
-1.63	5.59	212.8 (698.)	1.214 (.0023553)	790.4 (16.507)	.05795	.00280	.00063
-2.00	6.95	212.6 (698.)	1.218 (.0023642)	793.0 (16.561)	.06836	.00340	.00094
-2.25	8.34	212.6 (698.)	1.221 (.0023700)	781.9 (16.331)	.07810	.00398	.00121
-2.54	9.65	212.6 (698.)	1.223 (.0023721)	767.4 (16.027)	.08792	.00469	.00165
-2.81	****	212.9 (699.)	1.220 (.0023676)	753.5 (15.736)	.09614	.00533	.00190
-3.09	****	212.6 (698.)	1.216 (.0023592)	744.7 (15.554)	.09978	.00555	.00206
-3.37	6.74	212.7 (698.)	1.208 (.0023440)	802.8 (16.767)	.06401	.00286	.00070
-3.46	8.15	212.6 (698.)	1.206 (.0023392)	786.2 (16.420)	.07495	.00355	.00098
-.65	-.07	212.7 (698.)	1.217 (.0023610)	4.5 (.095)	.00165	-.00014	-.00001

(j) $Q \approx 1948\ N/m^2\ (40.7\ lb/ft^2)$, $CT \approx$ Variable

ALPHAC	TC(0)	VT	RHO	Q	----CONTROL---- CT	CH	CY
-.22	-.07	212.7 (698.)	1.216 (.0023599)	4.7 (.099)	.00043	.00002	-.00011
-1.07	4.46	212.3 (697.)	1.201 (.0023306)	1948.6 (40.697)	.05994	.00457	.00079
-2.12	4.28	212.5 (697.)	1.197 (.0023220)	1950.4 (40.736)	.05312	.00390	.00063
-2.09	4.78	212.5 (697.)	1.195 (.0023185)	1952.4 (40.777)	.06033	.00460	.00092
-2.06	5.30	212.6 (698.)	1.193 (.0023146)	1931.3 (40.336)	.06870	.00543	.00136
-.35	-.05	212.6 (698.)	1.211 (.0023500)	4.7 (.097)	.00081	.00005	-.00013

TABLE 1.- Concluded

(k) Q $\approx$ 1961 N/m^2 (40.5 lb/ft^2), CT $\approx$ Variable

ALPHAC	TC(0)	VT	RHO	Q	----CONTROL---- CT	CH	CY
-.23	-.05	213.1 (699.)	1.211 (.0023503)	4.7 (.099)	.00044	-.00003	-.00013
-6.60	5.88	212.5 (697.)	1.206 (.0023399)	1972.8 (41.203)	.04846	.00390	.00032
-6.53	6.90	212.2 (696.)	1.204 (.0023355)	1971.8 (41.182)	.06266	.00544	.00097
-6.45	7.92	212.6 (698.)	1.200 (.0023290)	1961.7 (40.972)	.07731	.00729	.00195
-6.37	8.94	212.1 (696.)	1.198 (.0023250)	1954.2 (40.814)	.08865	.00905	.00326
-6.33	9.47	212.6 (698.)	1.195 (.0023195)	1955.5 (40.843)	.09215	.00971	.00405

(l) Q $\approx$ 1961 N/m^2 (40.5 lb/ft^2), CT $\approx$ Variable

ALPHAC	TC(0)	VT	RHO	Q	----CONTROL---- CT	CH	CY
-8.55	6.45	212.7 (698.)	1.188 (.0023049)	1950.1 (40.729)	.03990	.00413	-.00030
-8.46	7.48	212.3 (697.)	1.191 (.0023117)	1946.4 (40.651)	.05425	.00545	.00021
-8.34	8.49	211.8 (695.)	1.197 (.0023218)	1959.3 (40.920)	.06908	.00721	.00096
-8.21	9.51	211.3 (693.)	1.199 (.0023255)	1958.4 (40.903)	.08212	.00916	.00196
-8.04	****	211.3 (693.)	1.201 (.0023302)	1965.2 (41.043)	.09099	.01079	.00331

(m) Q $\approx$ 2280 N/m^2 (47.6 lb/ft^2), CT $\approx$ Variable

ALPHAC	TC(0)	VT	RHO	Q	----CONTROL---- CT	CH	CY
-10.66	6.09	212.7 (698.)	1.196 (.0023210)	2280.8 (47.635)	.02415	.00332	-.00052
-10.60	7.11	212.1 (696.)	1.193 (.0023147)	2287.2 (47.770)	.03779	.00433	-.00015
-10.52	8.13	211.8 (695.)	1.191 (.0023105)	2282.7 (47.675)	.05272	.00578	.00045
-10.48	8.64	212.1 (696.)	1.184 (.0022979)	2277.7 (47.570)	.06044	.00672	.00078
-10.44	9.14	212.2 (696.)	1.183 (.0022963)	2275.4 (47.523)	.06761	.00773	.00114
-10.34	****	211.7 (695.)	1.182 (.0022927)	2272.3 (47.457)	.08082	.00999	.00223
-10.29	****	211.6 (694.)	1.180 (.0022903)	2270.5 (47.420)	.08506	.01083	.00297
-.52	-.05	212.7 (698.)	1.198 (.0023239)	4.5 (.095)	.00152	-.00001	-.00006

TABLE 2.- MODEL DATA

Number of blades	4
Airfoil section	NACA 0012
Radius, m (ft)	1.574 (5.167)
Chord, m (ft)	0.011 (0.353)
Twist, deg	0
Hinge offset, m (ft)	0.076 (0.25)
δ_3, deg	-2
Solidity	0.087

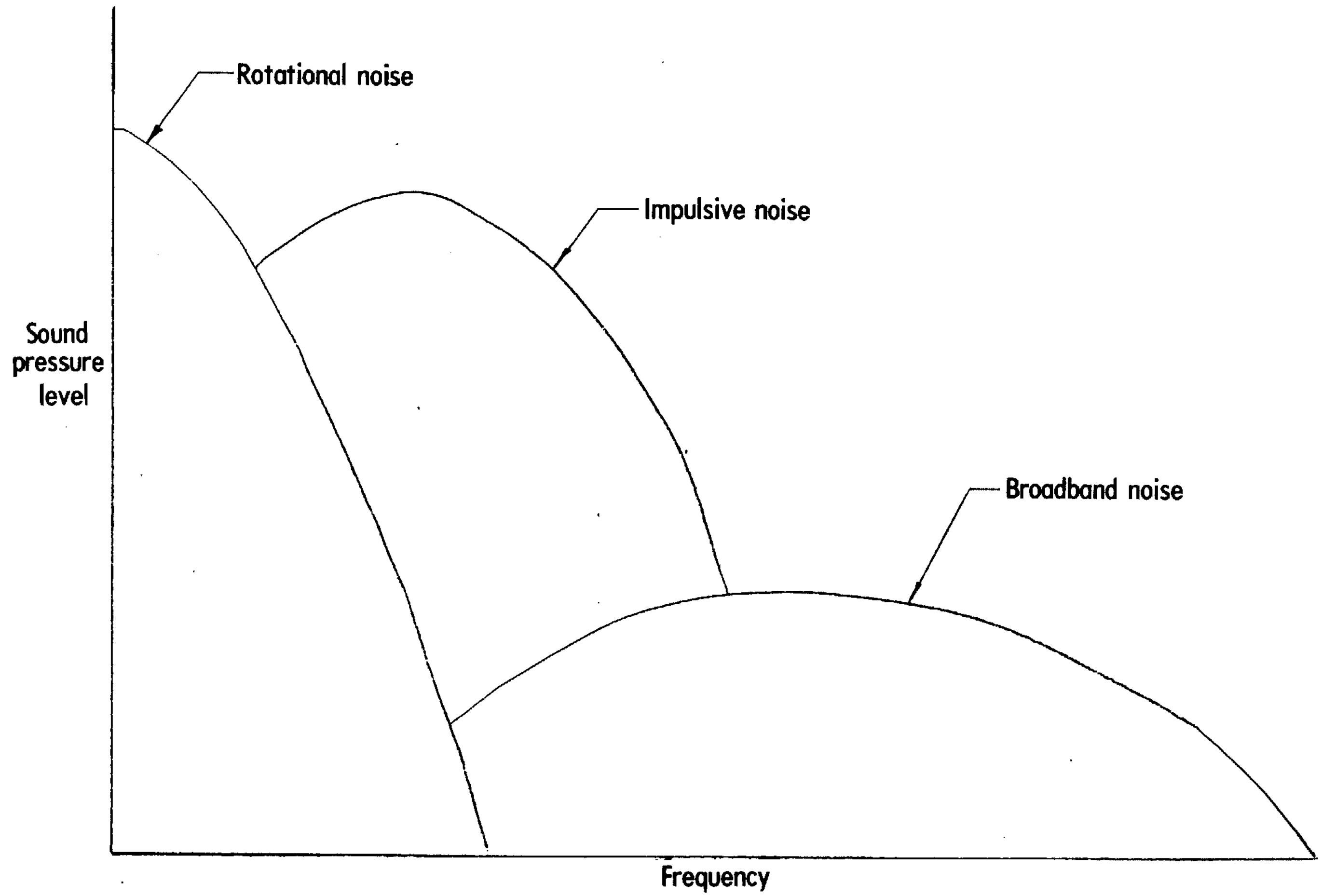

Figure 1.- Typical helicopter rotor acoustic spectrum.

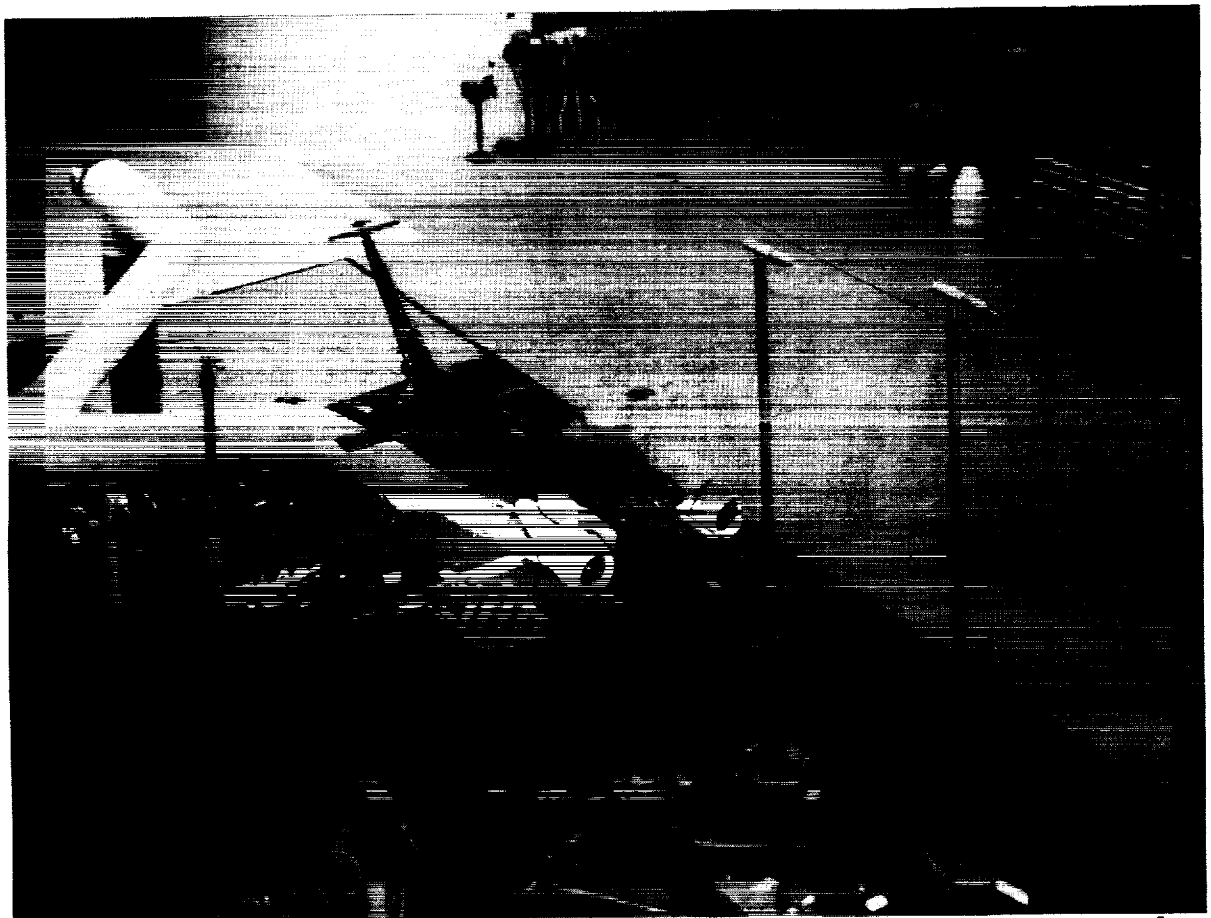

L-75-8951

Figure 2.- Helicopter model configuration used in acoustic tests.

MICROPHONE LOCATION			
mic no	x	y	z
1	279.0 (109.84)	-213.9 (-84.23)	297.1 (116.96)
2	133.7 (52.62)	-196.5 (-77.36)	297.2 (117.02)
3	386.1 (152.01)	-178.9 (-70.45)	296.9 (116.89)
4	355.8 (140.08)	+195.0 (+76.77)	297.8 (117.24)
5	128.9 (50.76)	+187.0 (+73.61)	297.5 (117.14)
6	453.0 (178.36)	+116.9 (+46.04)	297.6 (117.15)
7	242.4 (95.44)	-144.6 (-56.94)	(0) (0)
8	286.2 (112.69)	+129.2 (+50.88)	(0) (0)

ROTOR AXIS LOCATION AT α=0 ZERO REFERENCE		
x	y	z
307.7 (121.13)	0 (0)	292.0 (114.96)

TO COMPUTE ROTOR AXIS LOCATION AT VARIOUS α
IF $-2.4° < \alpha < 0$
x,cm = 307.7 - 60.6 sin (α + 2.4°)
{x,in. = 121.13 - 23.85 sin (α + 2.4°)}
ALL OTHER α
x,cm = 307.7 + 60.6 sin (α + 2.4°)
{x,in. = 121.13 + 23.85 sin (α + 2.4°)}
y = 0 (0)
z,cm = 231.5 + 60.6 cos (α + 2.4°)
{z,in. = 91.13 + 23.85 cos (α + 2.4°)}

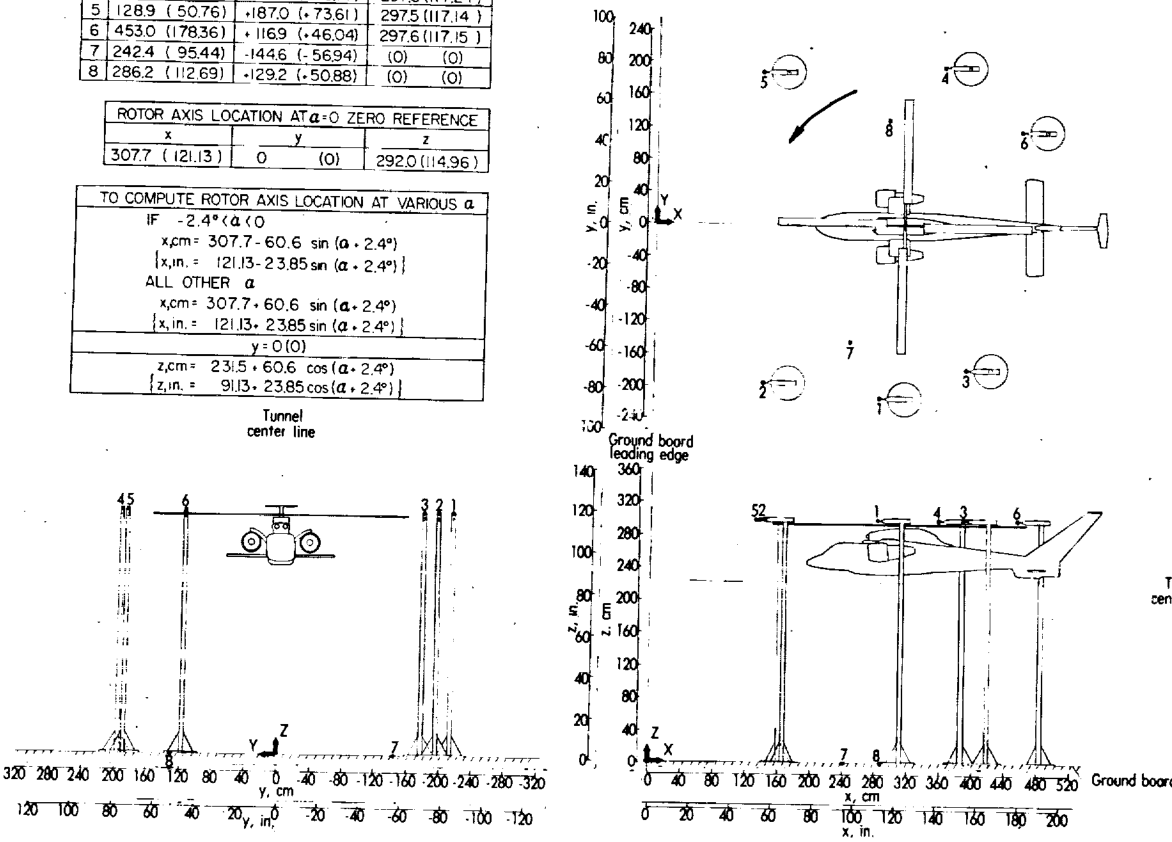

Figure 3.- Three-view drawing of general purpose research helicopter model and microphone arrangement. All dimensions in cm (in.).

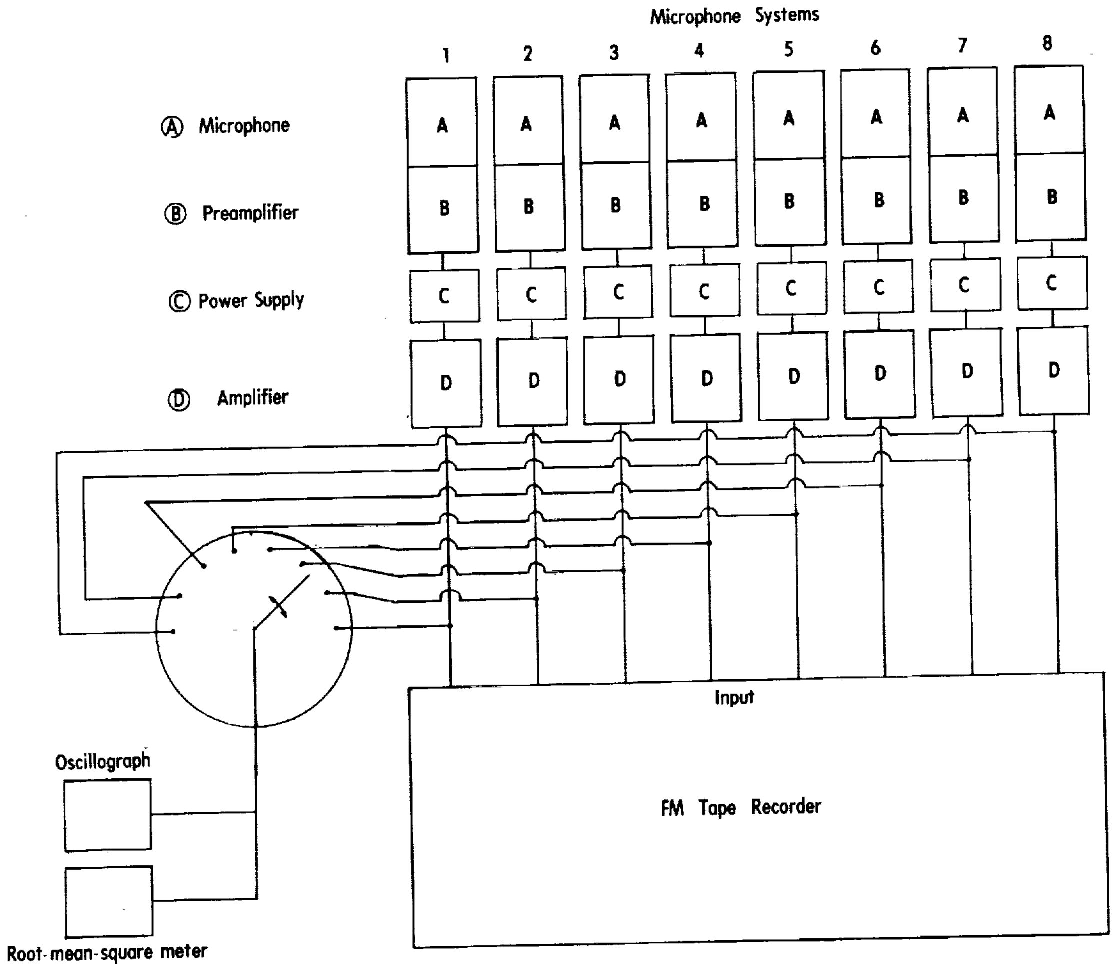

Figure 4.- Schematic of acoustic instrumentation and recording system.

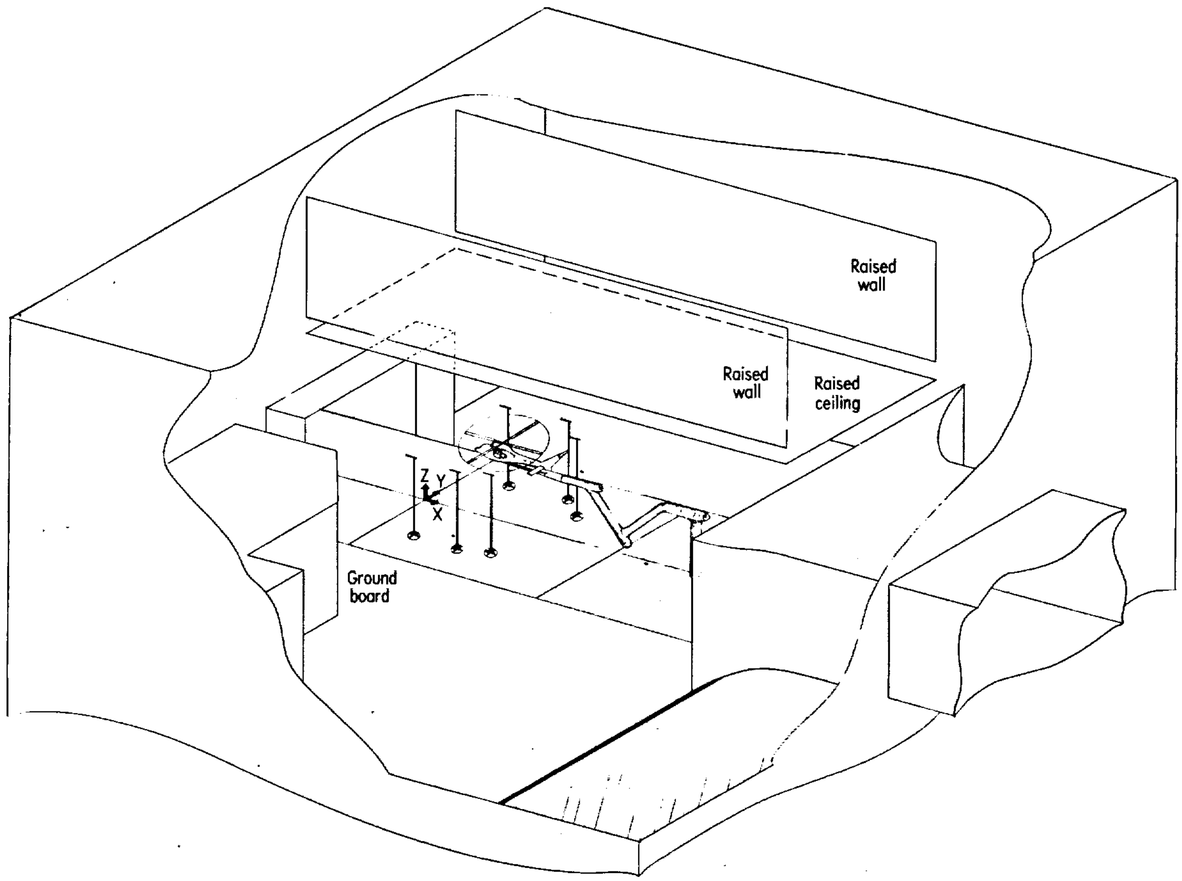

Figure 5.- Schematic of model in test chamber with microphone stands.

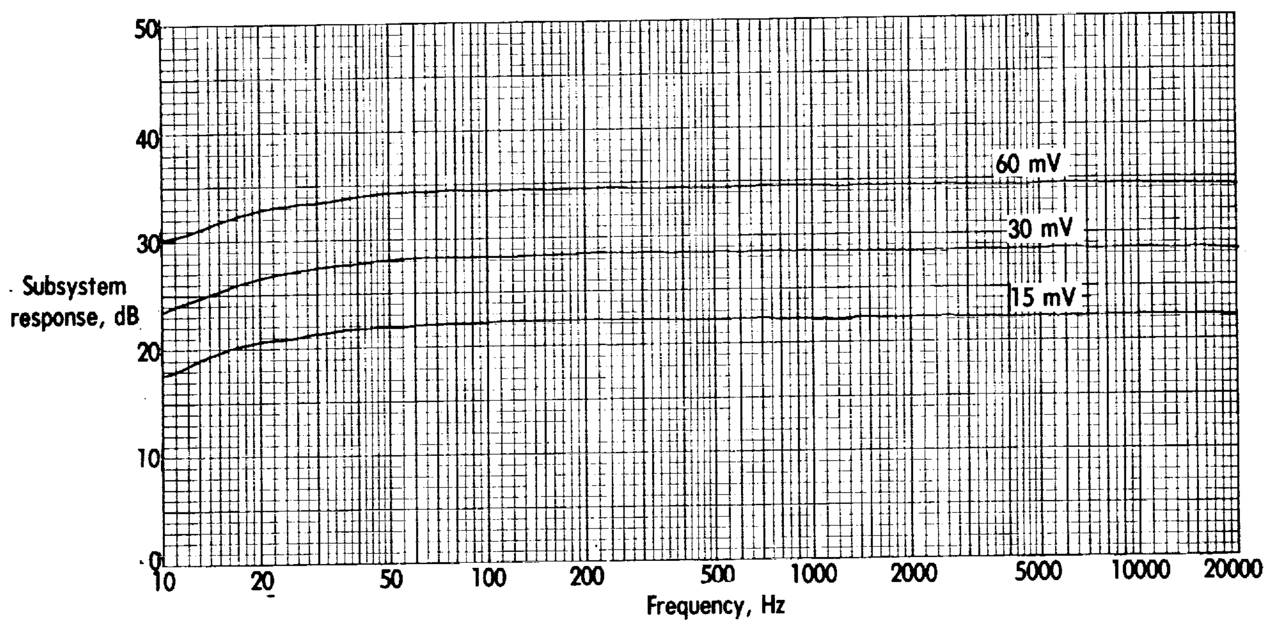

Figure 6.- Typical subsystem frequency response, including all equipment except the microphone and tape recorder.

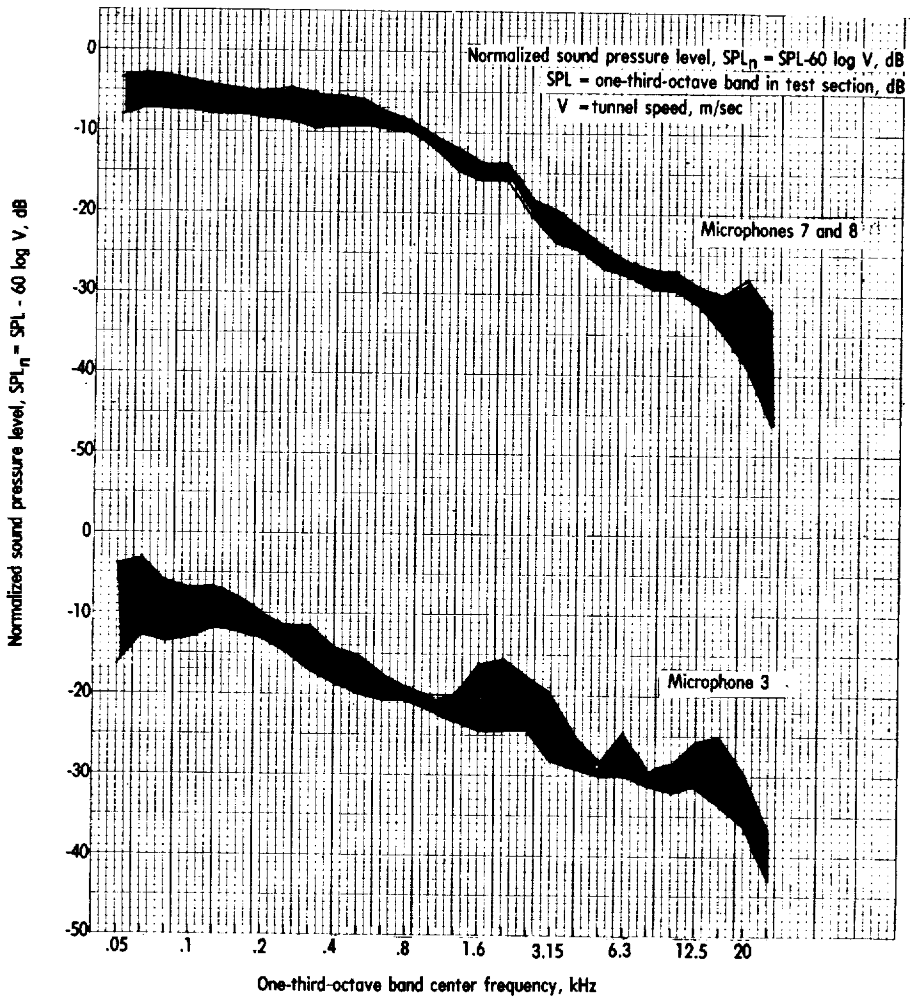

Figure 7.- Normalized background noise levels.

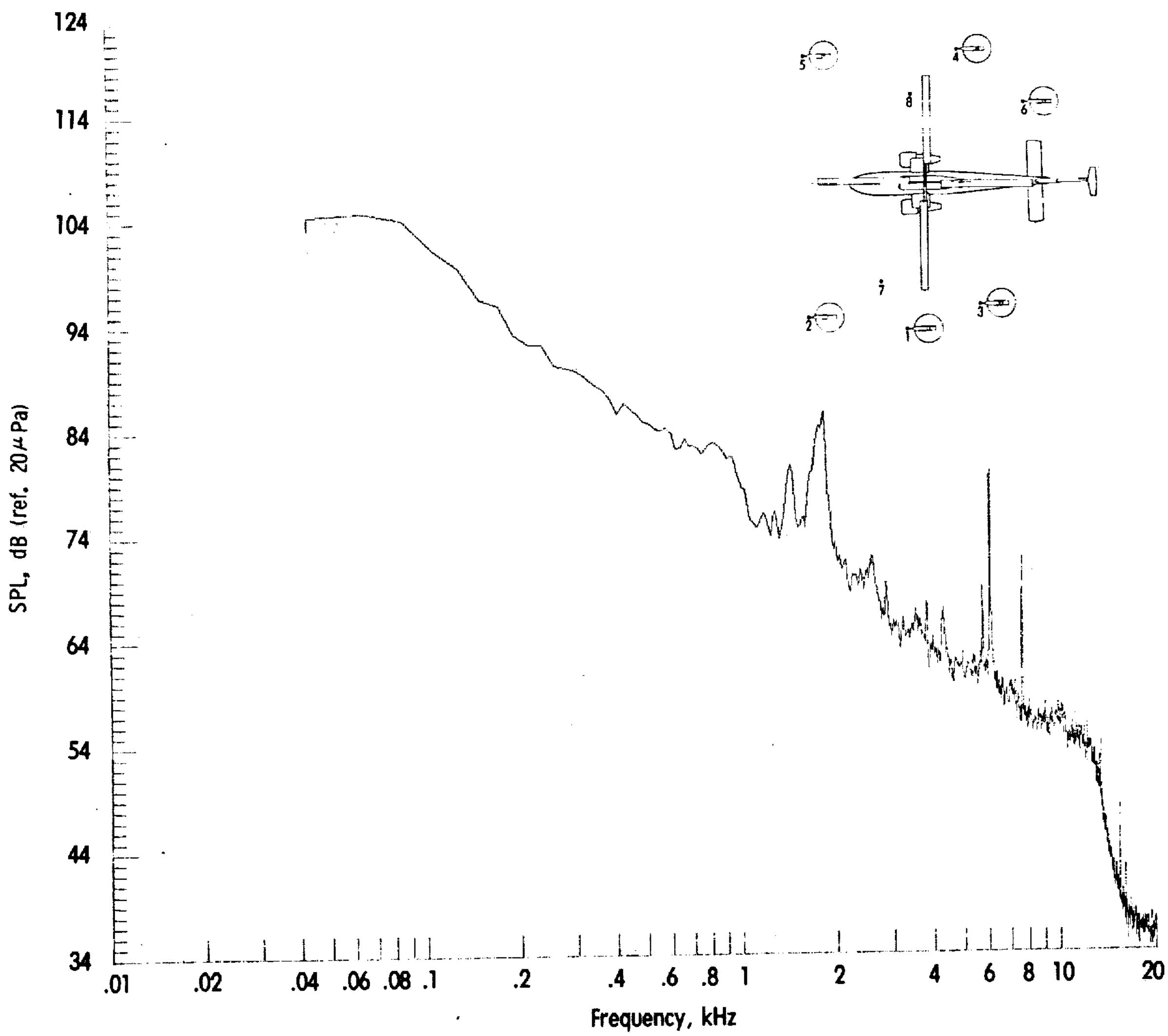

Figure 8.- Narrow band (12.5 Hz) spectrum of the background noise for microphone 3 at tunnel speed of 30.86 m/sec (99 ft/sec).

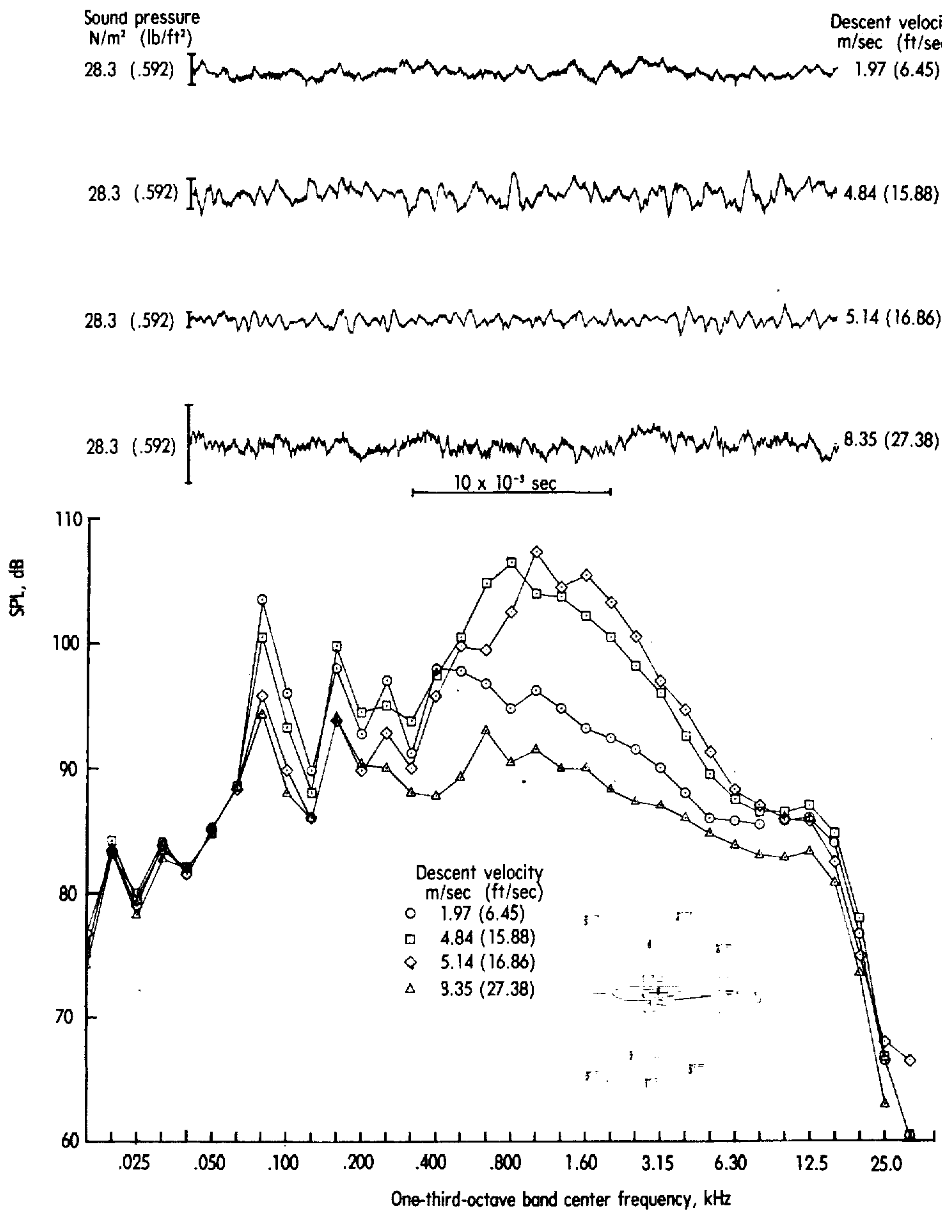

(a) Microphone 2.

Figure 9.- Oscillograph records and one-third-octave sound pressure level spectrum for various microphones and descent rates for a forward speed of 30.2 m/sec (99 ft/sec).

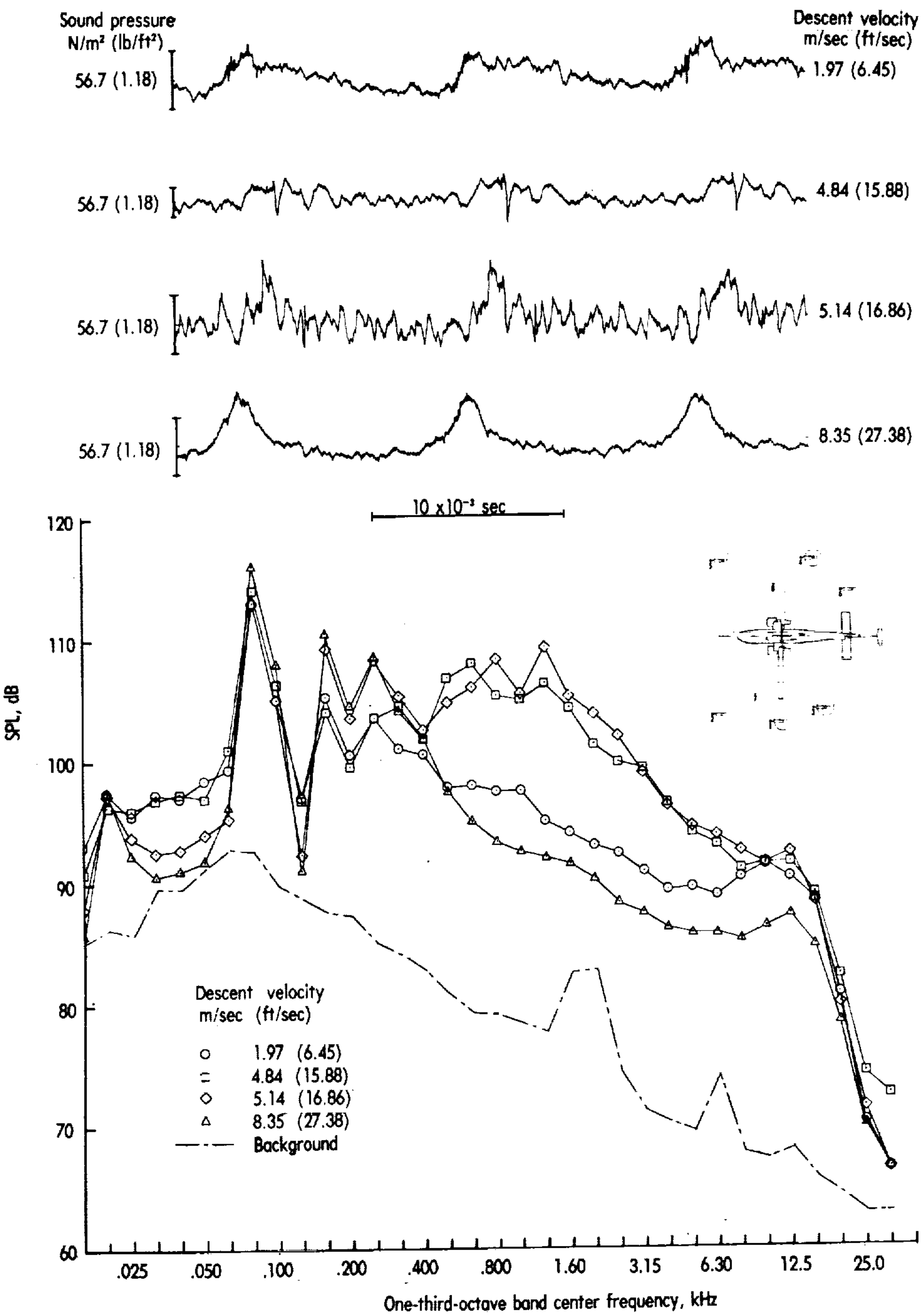

(b) Microphone 3.

Figure 9.- Continued.

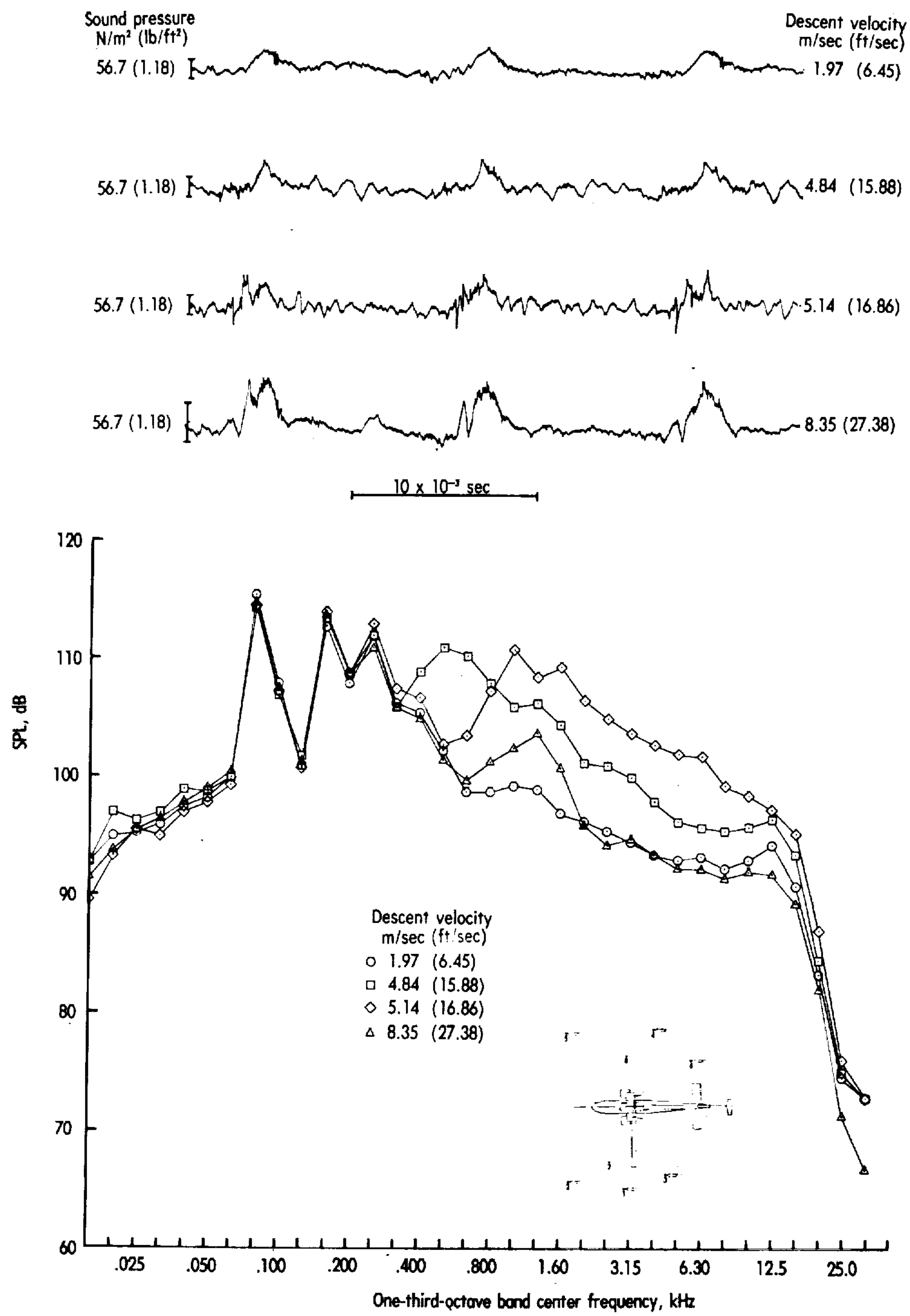

(c) Microphone 4.

Figure 9.- Continued.

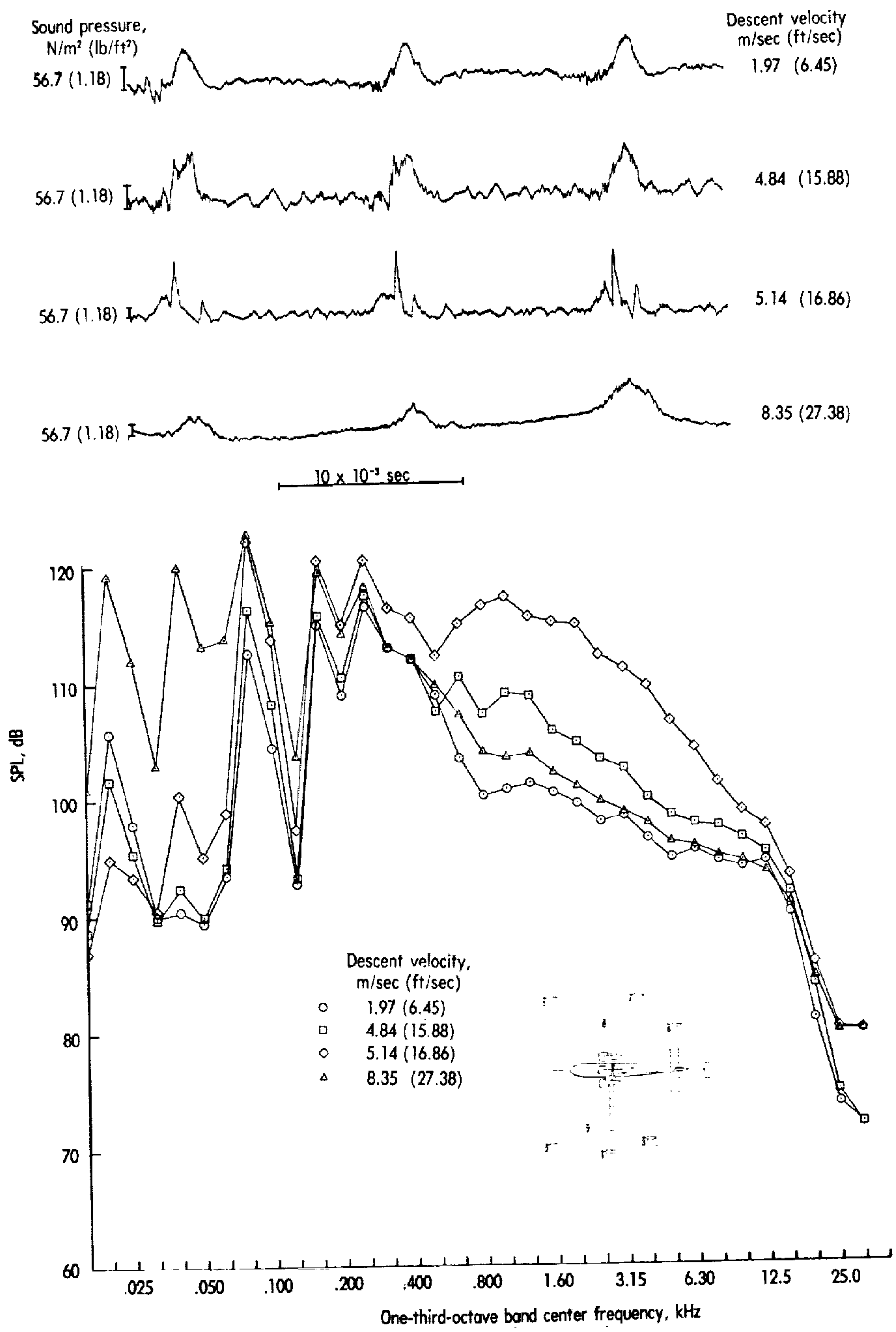

(d) Microphone 6.

Figure 9.- Continued.

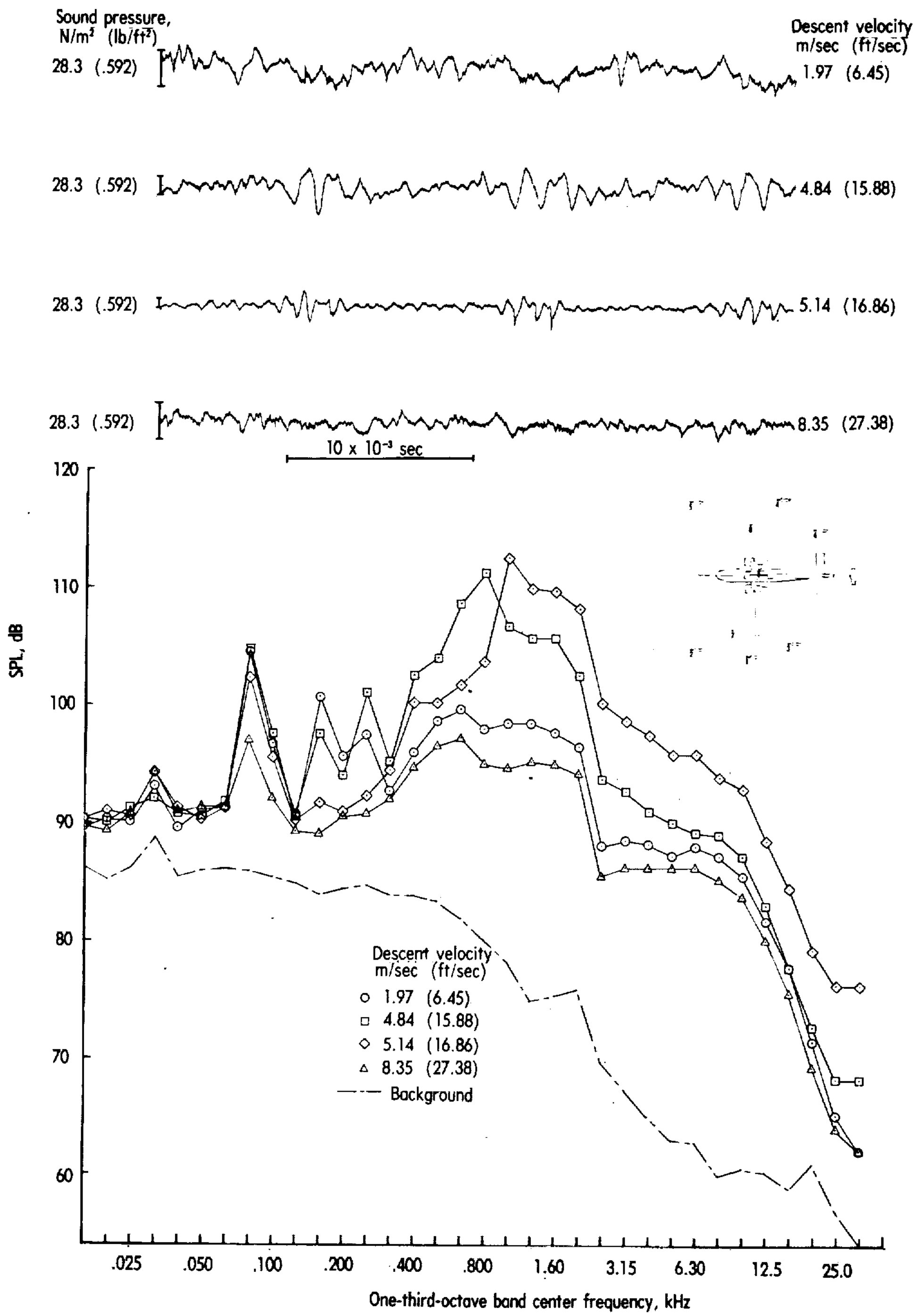

(e) Microphone 8.

Figure 9.- Concluded.

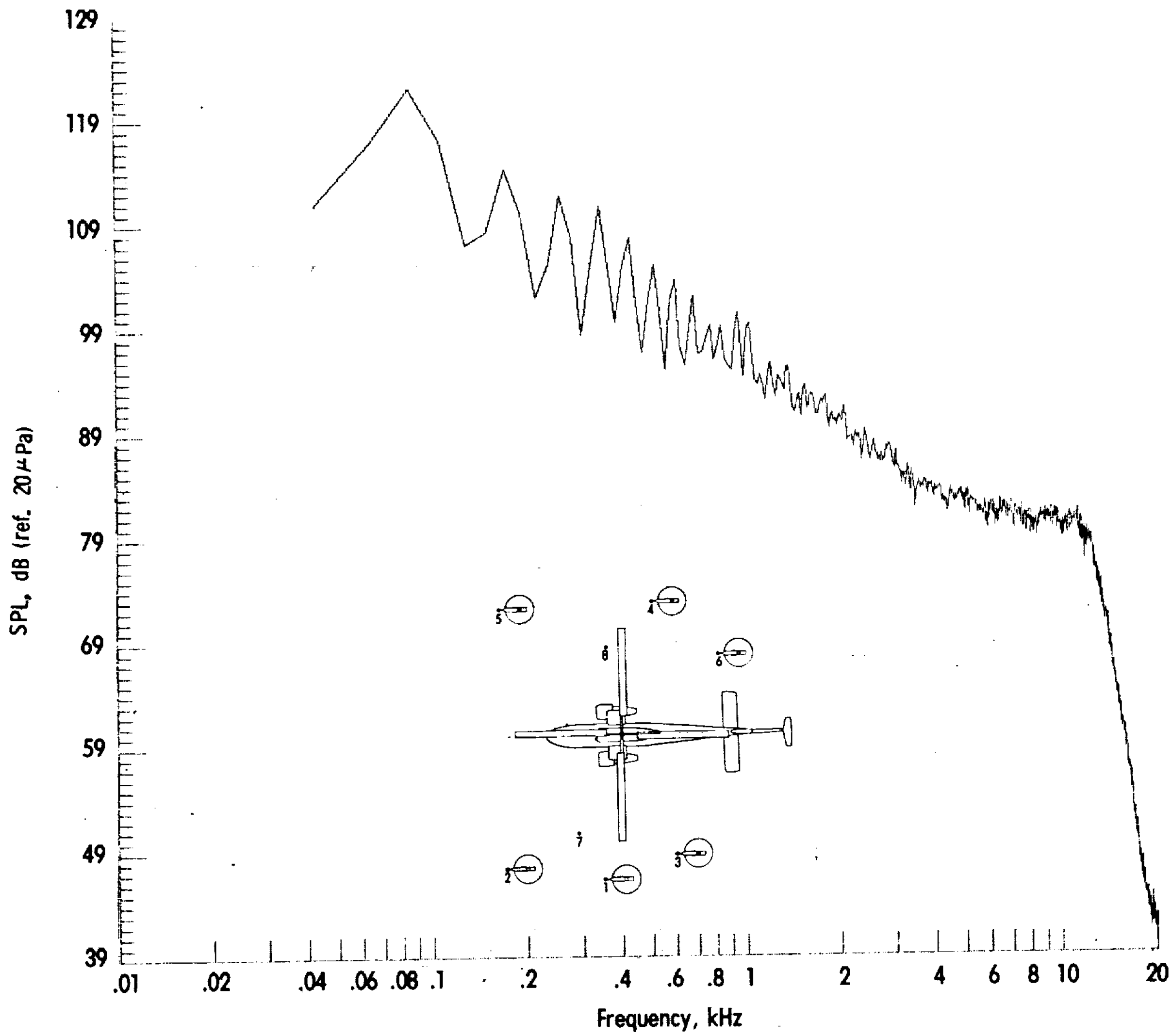

(a) Descent rate of 1.94 m/sec (6.45 ft/sec).

Figure 10.- Narrow-band sound pressure level spectrum for microphone 3, various descent rates, and a forward speed of 30.2 m/sec (99 ft/sec).

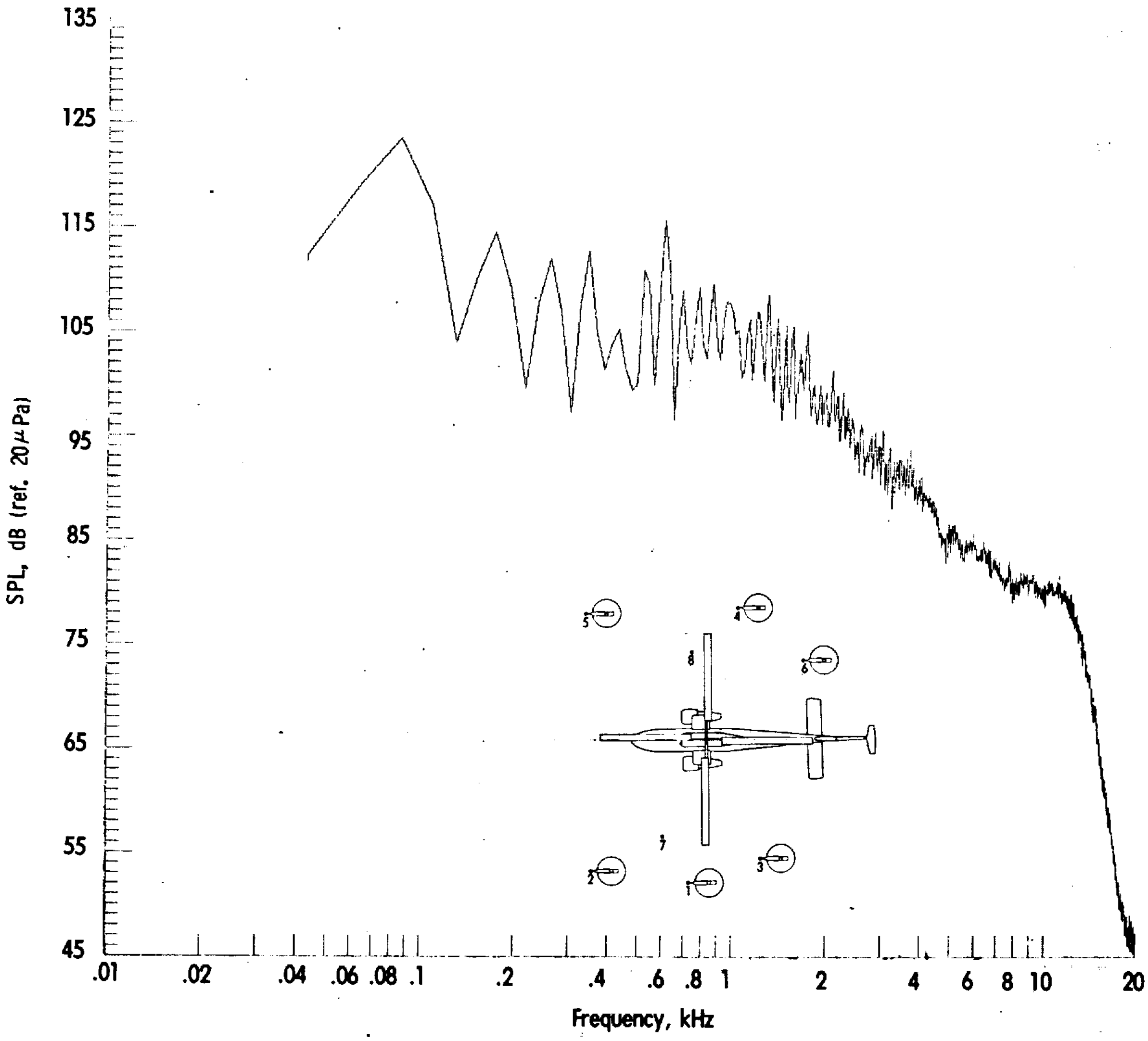

(b) Descent rate of 4.84 m/sec (15.88 ft/sec).

Figure 10.- Continued.

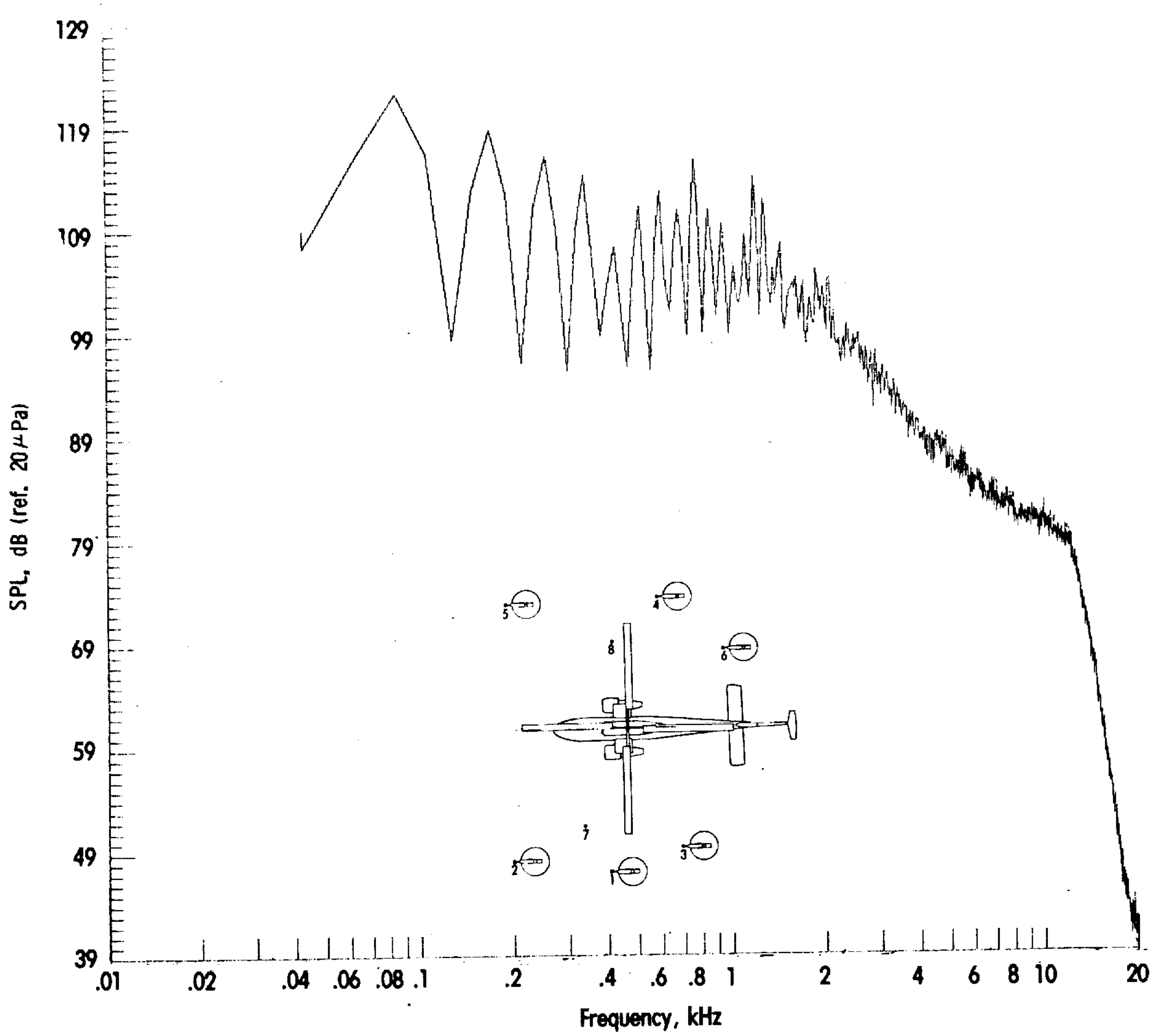

(c) Descent rate of 5.14 m/sec (16.9 ft/sec).

Figure 10.- Continued.

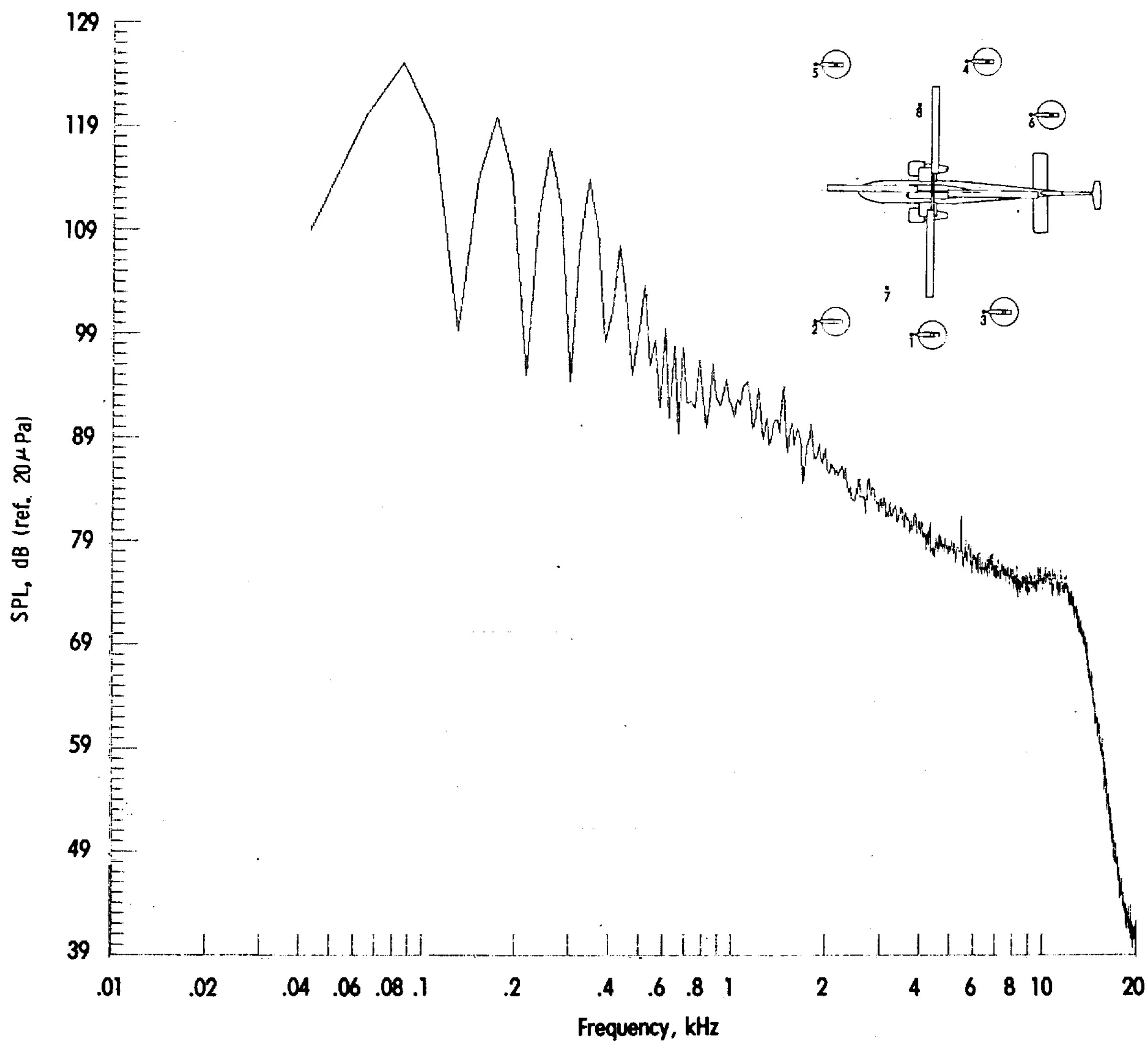

(d) Descent rate of 8.35 m/sec (27.4 ft/sec).

Figure 10.- Concluded.

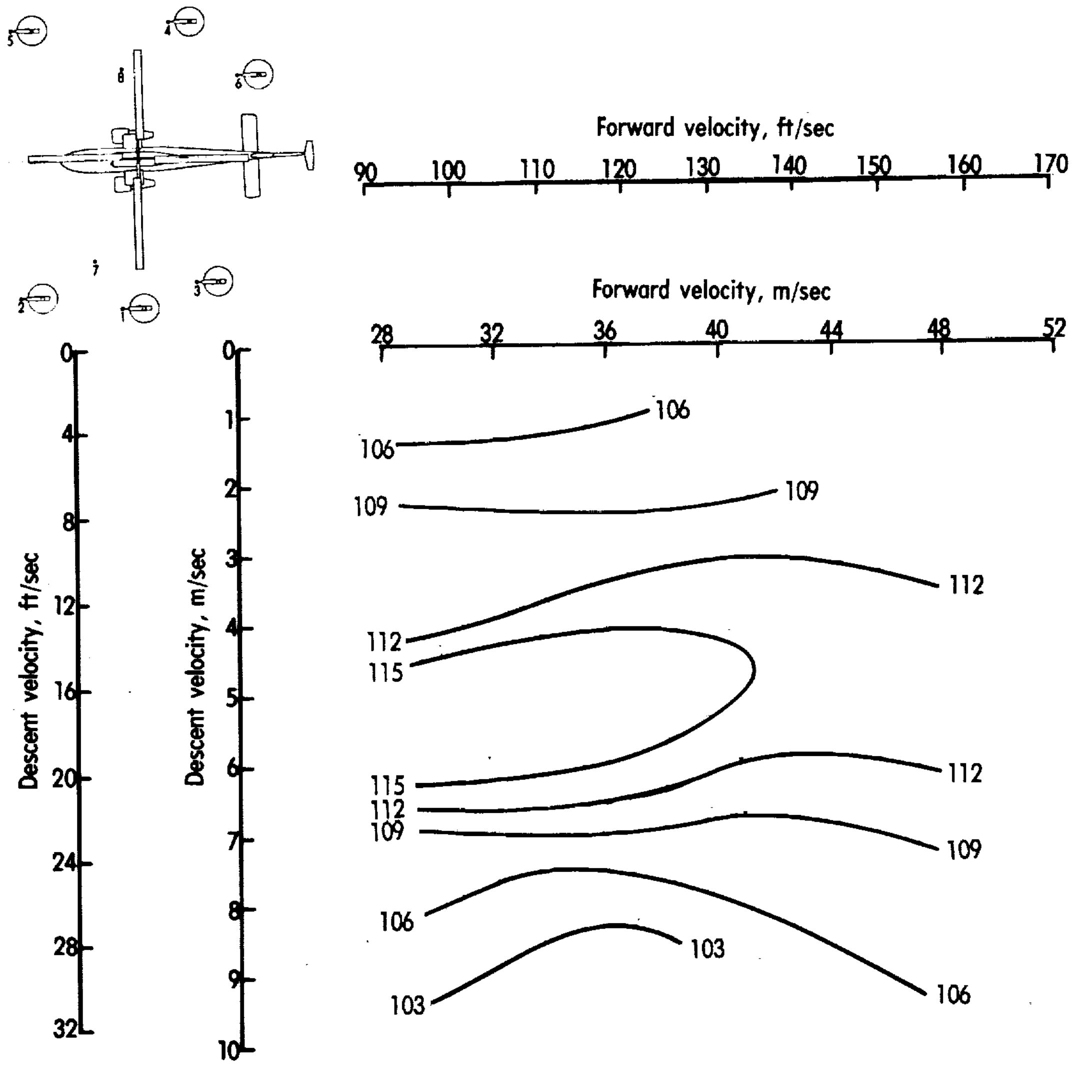

(a) Microphone 5.

Figure 11.- High-pass 500-Hz sound pressure level dB for various forward speeds, descent speeds, and microphone positions.

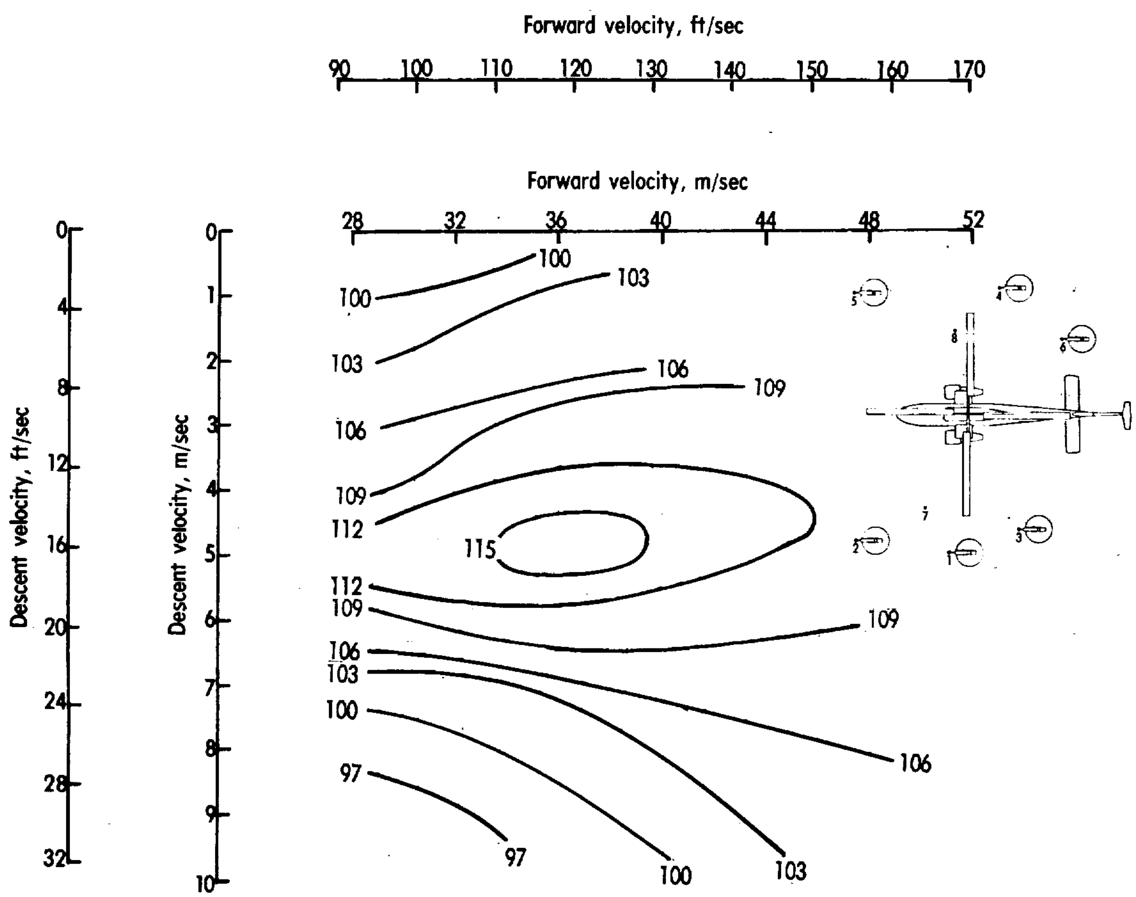

(b) Microphone 7.

Figure 11.- Concluded.

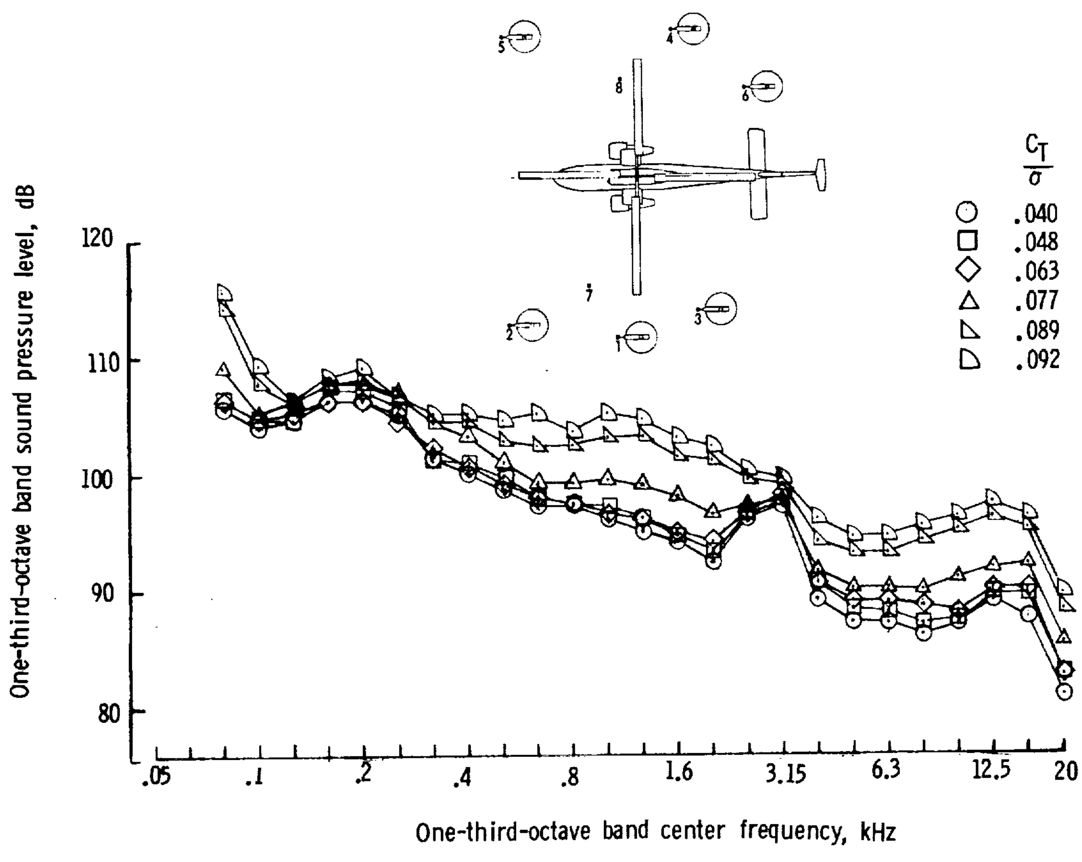

(a) Microphone 1.

Figure 12.- One-third-octave sound pressure level frequency spectrum for various microphone positions and thrust conditions. The forward speed is 56.6 m/sec (188 ft/sec) and the rotational speed is 213.4 m/sec (700 ft/sec).

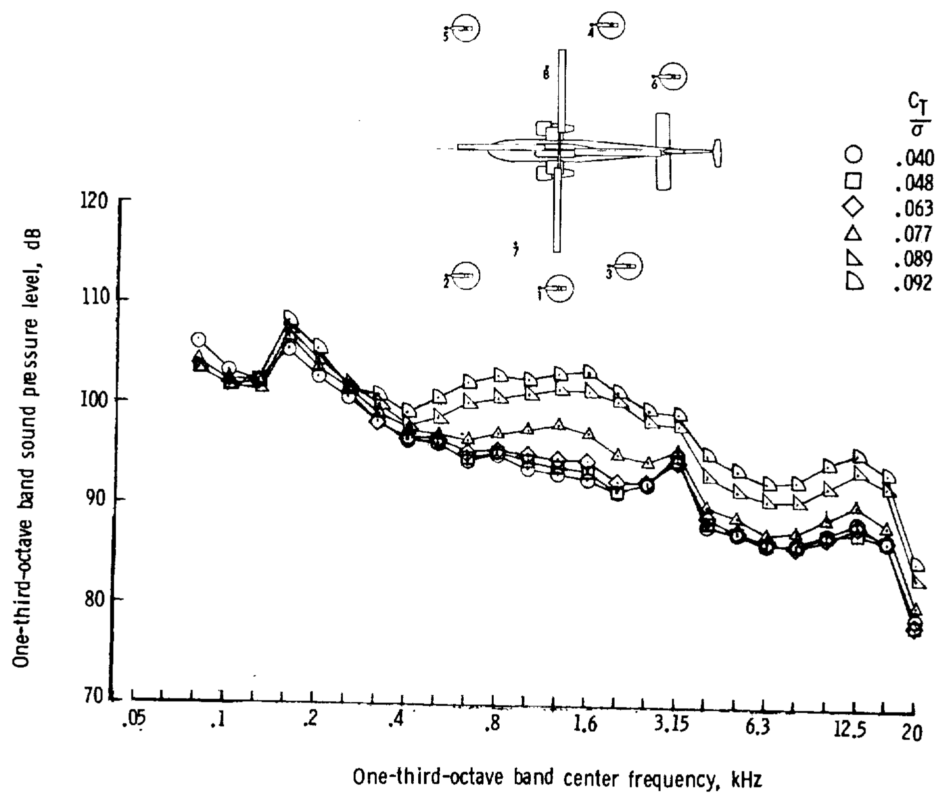

(b) Microphone 2.

Figure 12.- Continued.

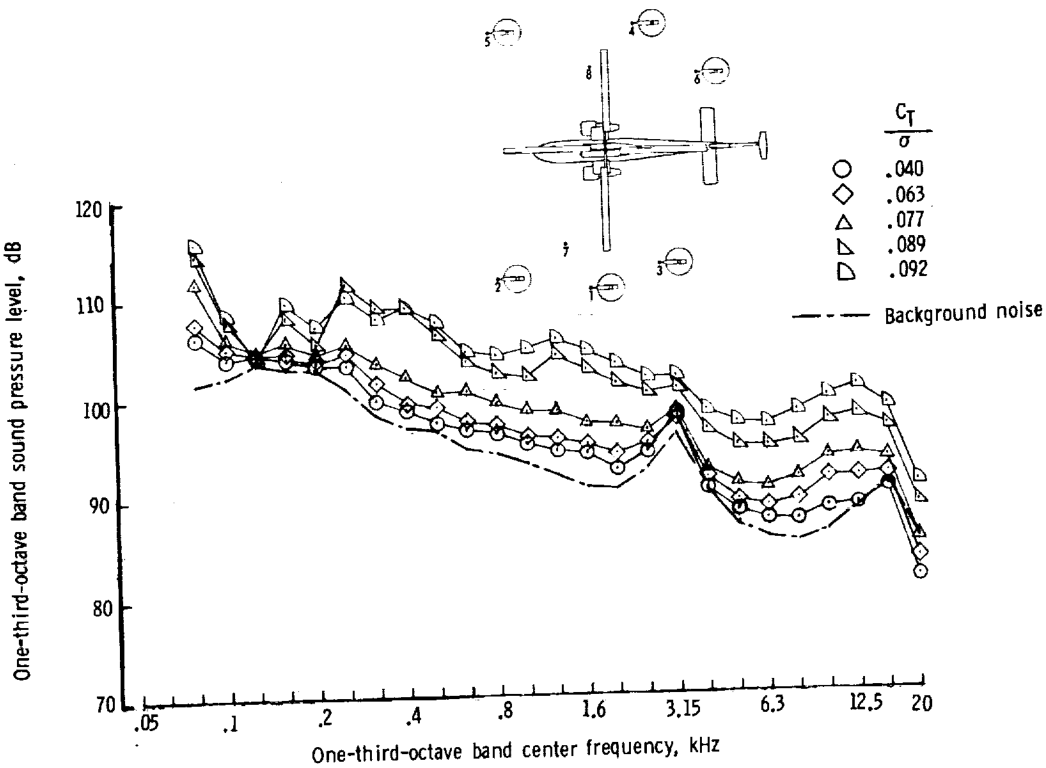

(c) Microphone 3.

Figure 12.- Continued.

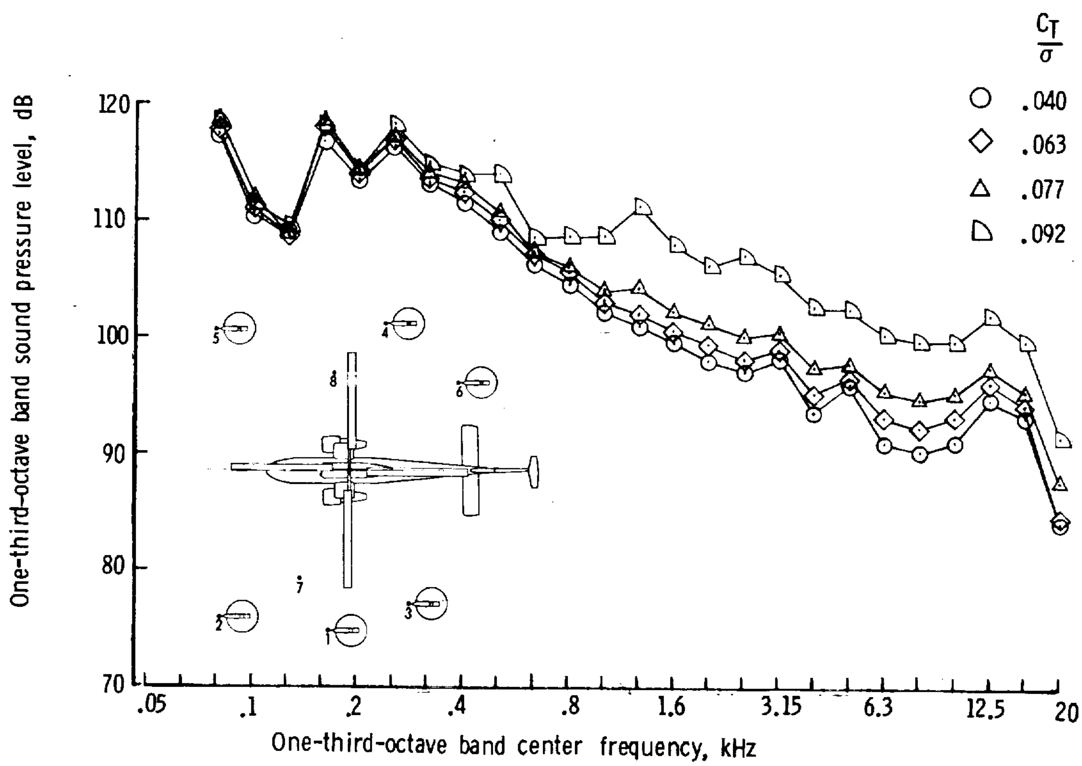

(d) Microphone 4.

Figure 12.- Continued.

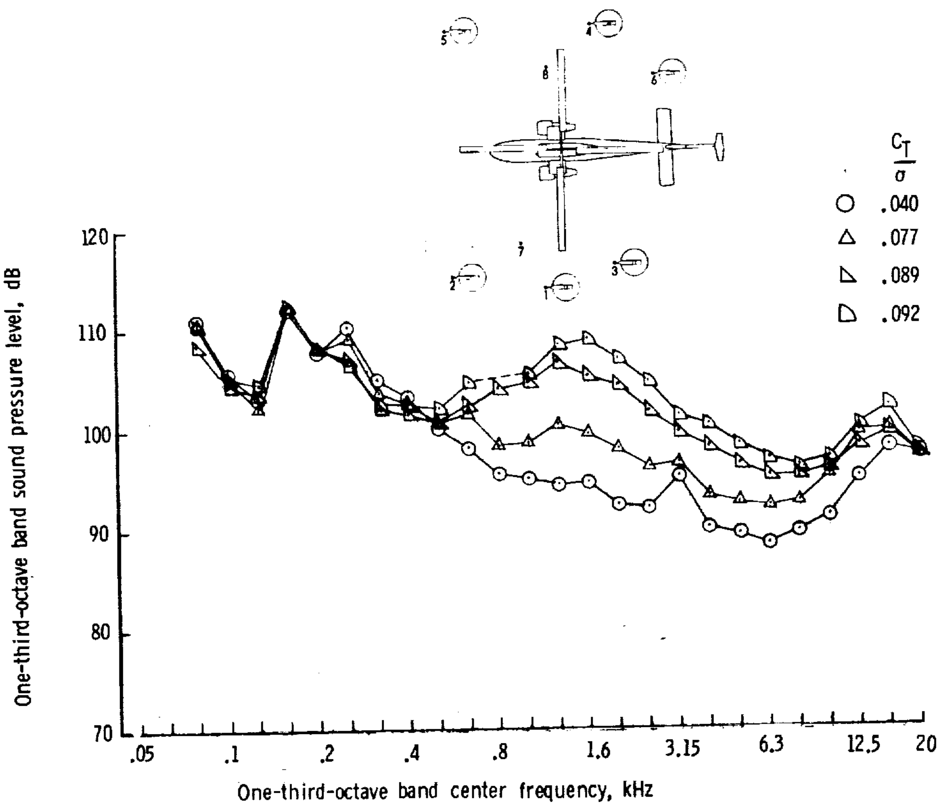

(e) Microphone 5.

Figure 12.- Continued.

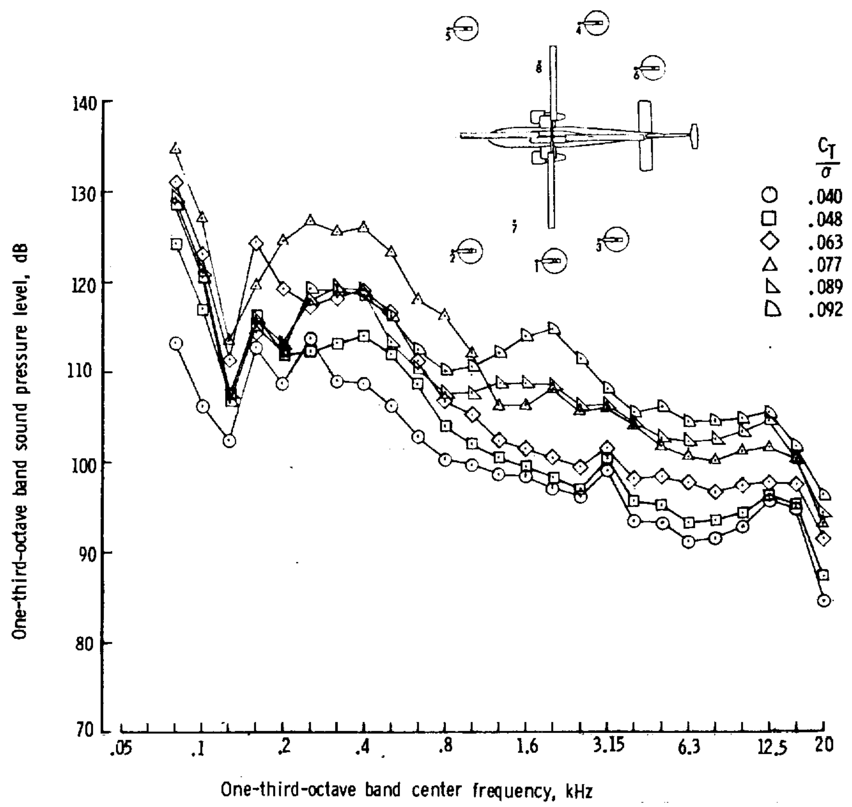

(f) Microphone 6.

Figure 12.- Continued.

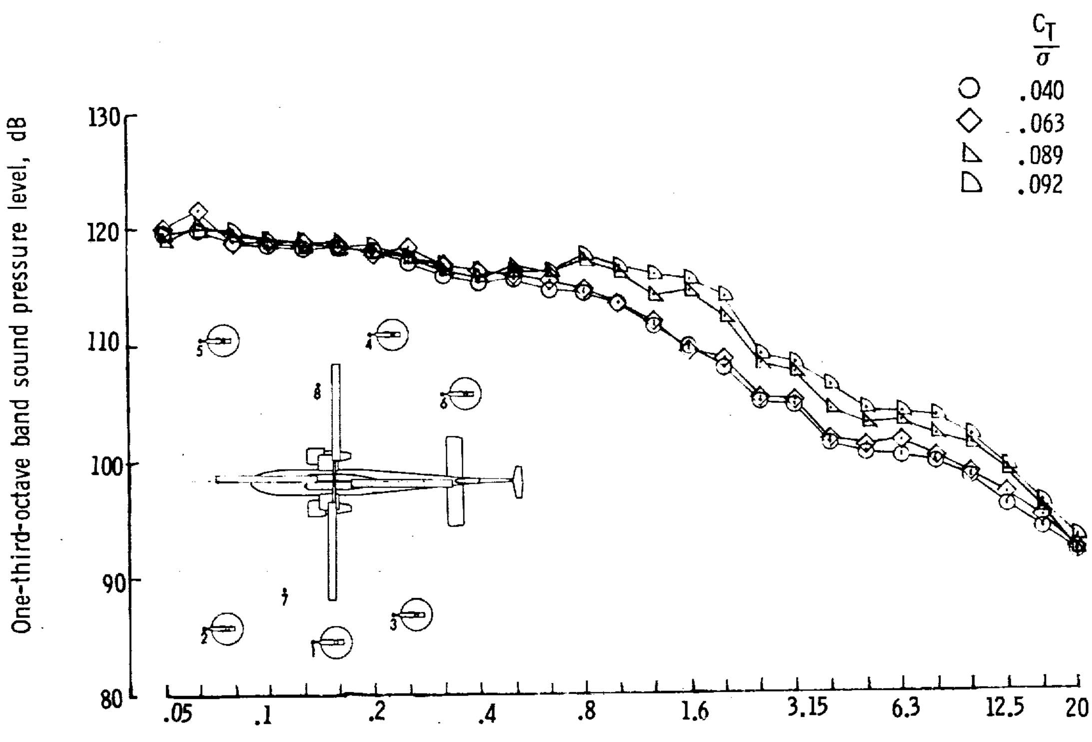

(g) Microphone 7.

Figure 12.- Continued.

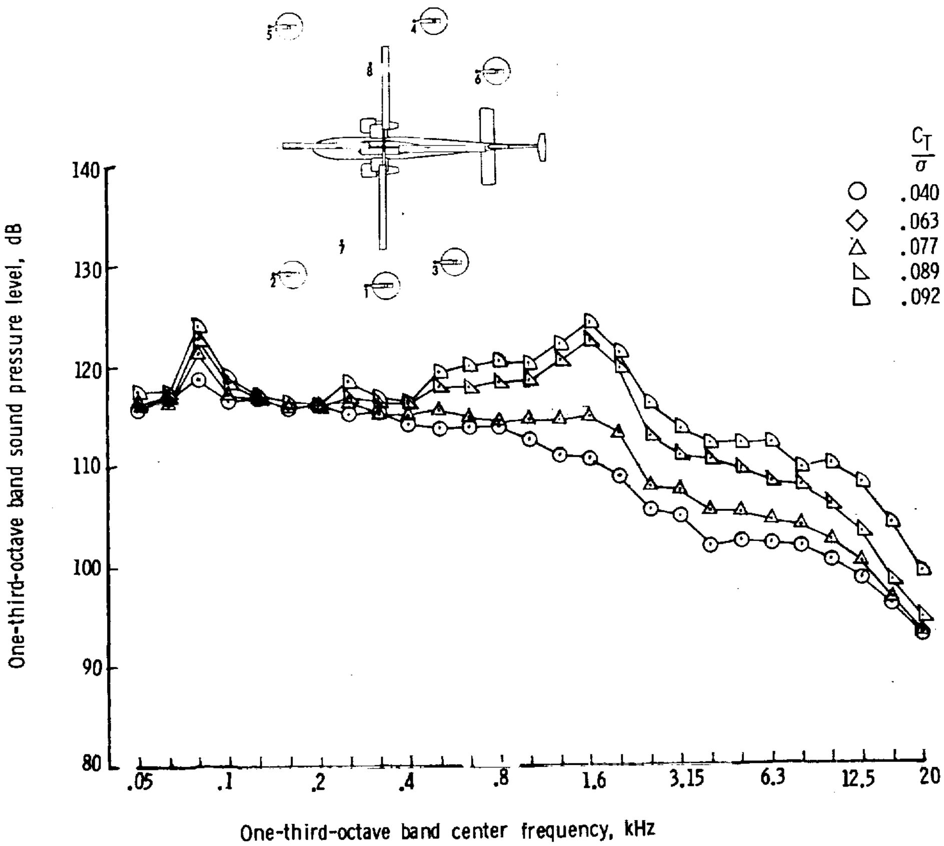

(h) Microphone 8.

Figure 12.- Concluded.

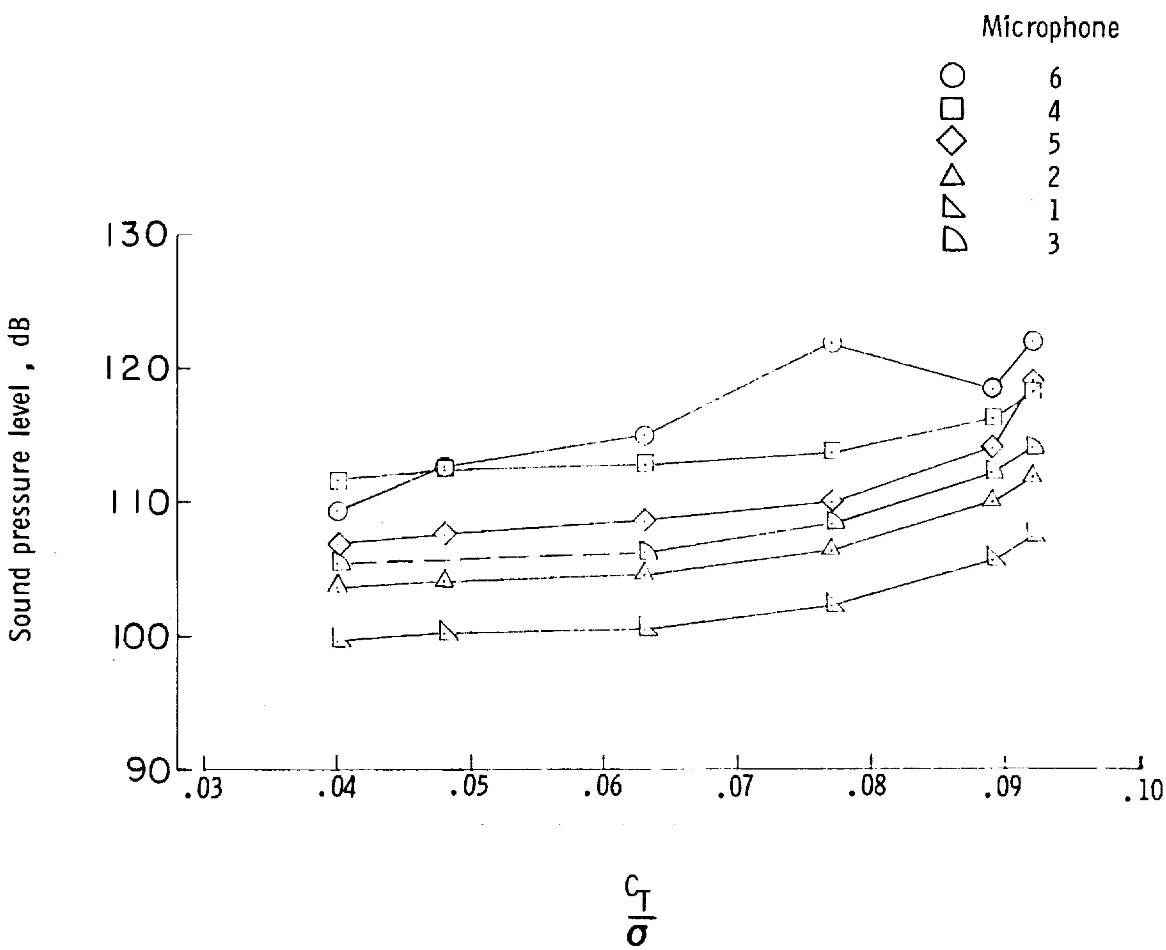

Figure 13.- 500-Hz high-pass filtered overall sound pressure levels as a function of rotor thrust values (C_T/σ) for various microphone positions and a forward speed of V = 56.6 m/sec (185.6 ft/sec).

NASA-Langley, 1977 L-11229